Pergamon

*Ocean Engng*, Vol. 23, No. 1, pp. 47–88, 1996

0029-8018/96 $9.50 + .00

0029-8018(95)00013-5

# SECOND-ORDER WAVEMAKER THEORY FOR IRREGULAR WAVES

Hemming A. Schäffer

Danish Hydraulic Institute, Agern Allé 5, DK-2970 Hørsholm, Denmark

(*Received for publication* 22 *October* 1994; *accepted* 30 *November* 1994)

**Abstract**—Through the last decade the theory for second-order irregular wave generation was developed within the framework of Stokes wave theory. This pioneering work, however, is not fully consistent. Furthermore, due to the extensive algebra involved, the derived transfer functions appear in an unnecessarily complicated form. The present paper develops the full second-order wavemaker theory (including superharmonics as well as subharmonics) valid for rotational as well as translatory wave board motion. The primary goal is to obtain the second-order motion of the wave paddle required in order to get a spatially homogeneous wave field correct to second order, i.e. in order to suppress spurious free-wave generation. In addition to the transfer functions developed in the line of references on which the present work is based, some new terms evolve. These are related to the first-order evanescent modes and accordingly they are significant when the wave board motion makes a poor fit to the velocity profile of the desired progressive wave component. This is, for example, the case for the high-frequency part of a primary wave spectrum when using a piston-type wavemaker. The transfer functions are given in a relatively simple form by which the computational effort is reduced substantially. This enhances the practical computation of second-order wavemaker control signals for irregular waves, and no narrow band assumption is needed. The software is conveniently included in a PC-based wave generation system—the DHI Wave Synthesizer. The validity of the theory is demonstrated for a piston type wavemaker in a number of laboratory wave experiments for regular waves, wave groups and irregular waves.

## 1. INTRODUCTION

First-order wavemaker theory corresponding to linearized Stokes theory has long been well established (Havelock, 1929; Biésel, 1951; Ursell *et al.*, 1960; and others; cf. the review by Svendsen, 1985) and we devote this introduction to second-order theories of wave generation.

The first step towards the development of wavemaker theory is of course the knowledge of the underlying wave theory. Already in 1847 Stokes gave results for regular waves in terms of a perturbation series using the wave steepness as the small ordering parameter. For regular waves only the sum frequencies appear (since the difference frequencies vanish) and Stokes found the resulting superharmonics.

Presumably the first approach to second-order wavemaker theory was given by Fontanet (1961) for regular waves. Using a Lagrangian description he found the spurious superharmonics generated by a purely sinusoidal oscillation of the wave board and gave directions as how to suppress these by adding a superharmonic component to the wavemaker control signal.

Hudspeth and Sulisz (1991) derived the complete second-order Eulerian theory waves generated by a monochromatic wave paddle motion with special emphasis on Stokes drift and return flow in wave flumes; see also Sulisz and Hudspeth (1993). This theory

has quite recently been extended to cover bichromatic paddle motion by Moubayed and Williams (1994). The theories of Fontanet, Hudspeth and Sulisz, and Mobayed and Williams appear to be the most complete theoretical developments yet.

Madsen (1971) developed an approximate theory for the suppression of spurious superharmonics in regular waves generated in fairly shallow water.

Buhr Hansen *et al.* (1975) chose an empirical approach to pursue the second-order control signal for regular waves. The second-order regular wave field generated by a first-order control signal has further been studied by Flick and Guza (1980).

For irregular waves both sum and difference frequencies appear in the interaction terms at second order. Longuet-Higgins and Stewart (1962, 1964) derived results for the subharmonics with the restriction of only slightly different frequencies (narrow band restriction) in the interacting wave components. Without this restriction Ottesen-Hansen (1978) gave similar results in a more suitable form, i.e. using a transfer function giving the second-order contribution in terms of the interacting first-order wave components. A generalization including both subharmonics and superharmonics for directional waves was given by Sharma (1979); see also Dean and Sharma (1981).

Neglecting the evanescent modes in the first-order solution, Flick and Guza (1980) gave an approximate theory for the generation of spurious long waves by a first-order bichromatic control signal under the narrow band assumption.

Without this assumption Sand (1982) calculated the second-order subharmonic control signal for a piston-type wavemaker needed to suppress spurious long wave generation. A more detailed description of the theory was given by Barthel *et al.* (1983), who also extended the theory to include a rotating wave board motion, restricting the centre of rotation to a point at or below the bottom. This is, however, an inconvenient restriction, since many wavemakers are equipped with a hinge situated above the bottom. Sand and Donslund (1985) gave the required theoretical extension.

For irregular waves a technique for the synthesis of wavemaker control signals based on the narrow band assumption for the first-order carrier waves has further been used by Klopman and Van Leeuwen (1990) and by Bowers (1988) (discussed by Mansard *et al.*, 1989) for subharmonic frequencies. This approximation allows for an efficient time–domain computation of the second-order control signal.

For irregular waves Sand and Mansard (1986a,b) derived the wavemaker theory for the superharmonics valid for translatory as well as rotating wave boards. For a directional wavemaker Suh and Dalrymple (1987) developed part of the theory for the spurious superharmonic and subharmonic second-order waves generated by a first-order wavemaker control signal.

In the present paper the full second-order wavemaker theory is rederived in a unifying and compact form that includes both superharmonics and subharmonics and covers wavemakers of the piston and hinged type.† Following the line of Sand and his co-workers the primary goal is to obtain the second-order motion of the wave paddle required in order to get a spatially homogeneous wave field correct to second order, i.e. in order to suppress spurious free-wave generation. As in Sand's work, this is done without assuming the primary waves to be restricted by a narrow frequency band.

† Inconsistencies in the previous derivations are pointed out concurrently using footnotes.

In order to facilitate and reduce the theoretical calculations, a complex representation is chosen, although the resulting transfer functions are also given in real form.

For a piston-type wavemaker, the theory is verified in a number of experiments with regular waves, wave groups and irregular waves, respectively.

A first version of this theory was presented at an SUT conference (Schäffer, 1993a). Compared with the present formulation, it included a formal solution to the problem of second-order wave generation in a more general form as regards the type of wavemaker considered. However, it can be shown that for some of these wavemakers the solution includes divergent series and in the present formulation these types are not considered.

## 2. GENERAL THEORY

### 2.1. *Governing equations*

The classical method of perturbation theory in combination with Taylor expansions of the boundary conditions at the free surface and at the wave board leads to a boundary-value problem for the first- and second-order wave contributions, respectively (Stokes, 1847; Flick and Guza, 1980; and others). Let $(u, w) = (\Phi_x, \Phi_z)$ define the velocity potential $\Phi = \Phi(x, z, t)$ in a Cartesian coordinate system $(x, z)$, cf. Fig. 1, and let $\eta = \eta(x, t)$, $X = X(z, t)$, $g$, $h$, and $t$ denote surface elevation, wave board position, acceleration of gravity, still water depth, and time, respectively, then the relevant boundary-value problems may be written

$$\Delta\Phi = 0 \qquad \text{everywhere} \tag{1a}$$

$$\Phi_{tt} + g\Phi_z = R \qquad \text{for } z = 0 \tag{1b}$$

$$\Phi_x = Q \qquad \text{for } x = 0 \tag{1c}$$

$$\eta = \frac{1}{g}(\Phi_t + P) \qquad \text{for } z = 0 \tag{1d}$$

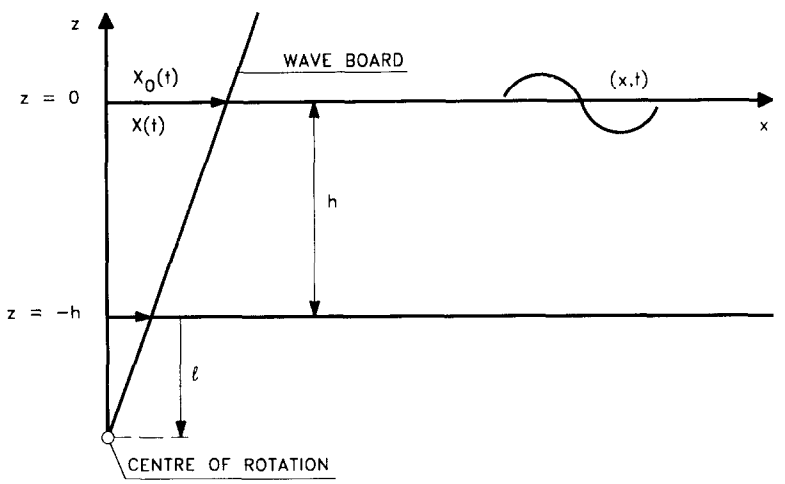


Fig. 1. Definition sketch [the wave board motion indicated corresponds to Fig. 2(b)].

$$\Phi_z = 0 \qquad \text{for } z = -h, \tag{1e}$$

where $R$, $Q$ and $P$ are given below. The elevation, potential and wave board position [see Equation (5)] correct to second order are given by

$$\eta = \epsilon\eta^{(1)} + \epsilon^2 \eta^{(2)} \tag{2a}$$

$$\Phi = \epsilon\Phi^{(1)} + \epsilon^2 \Phi^{(2)} \tag{2b}$$

$$X_0 = \epsilon X_0^{(1)} + \epsilon^2 X_0^{(2)}\,, \tag{2c}$$

where $\epsilon$ is a small ordering parameter, and (1) covers the first-order problem for $(\Phi, \eta) = (\Phi^{(1)}, \eta^{(1)})$, where

$$R^{(1)} = 0 \tag{3a}$$

$$Q^{(1)} = f(z)\, X_{0t}^{(1)} \tag{3b}$$

$$P^{(1)} = 0 \tag{3c}$$

and the second-order problem for $(\Phi, \eta) = (\Phi^{(2)}, \eta^{(2)})$, where†

$$R^{(2)} = -\left\{(\Phi_x^{(1)2} + \Phi_z^{(1)2})_t + \eta^{(1)}(\Phi_{tt}^{(1)} + g\Phi_z^{(1)})_z\right\} \tag{4a}$$

$$Q^{(2)} = \begin{cases} -X_0^{(1)}\{f(z)\,\Phi_{xx}^{(1)} - \dfrac{1}{h+l}\Phi_z^{(1)}\} + f(z)\, X_{0t}^{(2)} & \text{for } -(h-d) \le z \le 0 \\ 0 & \text{for } -h \le z < -(h-d) \end{cases} \tag{4b}$$

$$P^{(2)} = \frac{1}{2}\left(\Phi_x^{(1)2} + \Phi_z^{(1)2}\right) + \eta^{(1)}\Phi_{zt}^{(1)}\,. \tag{4c}$$

The position of the wave board is

$$X(z,t) = f(z)\, X_0(t) \tag{5}$$

where $f(z)$ describes the type of wavemaker:

$$f(z) = \begin{cases} 1 + \dfrac{z}{h+l} & \text{for } -(h-d) \le z \le 0 \\ 0 & \text{for } -h \le z < -(h-d)\,. \end{cases} \tag{6}$$

Here $z = -(h + l)$ gives the centre of rotation ($-h < l \le \infty$) and $d \ge 0$ is the elevation of the hinge over the bottom, i.e. $d = -l$. If the centre of rotation is at or below the bottom, then $d = 0$ and the last case in Equation (6) becomes irrelevant. Figure 2 shows the types of wavemakers considered. Thus we have made the restriction that either $d = -l$ or $d = 0$, $l \ge 0$. This ensures that only continuous shape functions $f(z)$

† For wave boards hinged above the bottom, $Q = 0$ must be required specifically below the hinge. The consequence of this fact was not fully drawn in Sand and Donslund (1985) and Sand and Mansard (1986a,b).

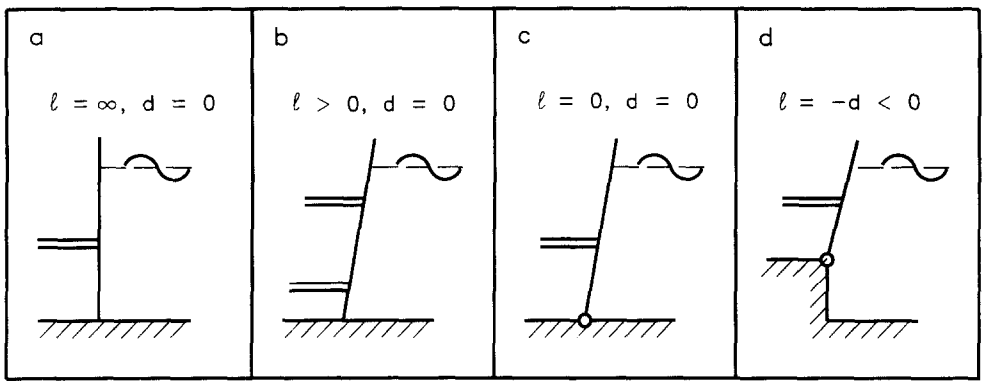


Fig. 2. The theory is developed for these types of wave board motions: (a) translatory (piston type) and (b)–(d) rotational with the centre of rotation (b) below, (c) at, and (d) above the bottom.

are considered, and it can be shown to be a necessary condition for the convergence of the infinite series that appear in the second-order wavemaker theory.

As described in detail by Barthel *et al.* (1983), the second-order problem is conveniently separated into three contributions:

$$\Phi^{(2)} = \Phi^{(21)} + \Phi^{(22)} + \Phi^{(23)} \tag{7a}$$

$$\eta^{(2)} = \eta^{(21)} + \eta^{(22)} + \eta^{(23)} \tag{7b}$$

and the respective boundary-value problems are given by Equation (1), where for $(\Phi, \eta) = (\Phi^{(21)}, \eta^{(21)})$:

$$R^{(21)} = -\left\{\left(\Phi_x^{(1)^2} + \Phi_z^{(1)^2}\right)_t + \eta^{(1)}\left(\Phi_{tt}^{(1)} + g\Phi_z^{(1)}\right)_z\right\} \tag{8a}$$

$$Q^{(21)} = \text{arbitrary (i.e. condition disappears)} \tag{8b}$$

$$P^{(21)} = \frac{1}{2}\left(\Phi_x^{(1)^2} + \Phi_z^{(1)^2}\right) + \eta^{(1)}\Phi_{zt}^{(1)} \tag{8c}$$

for $(\Phi, \eta) = (\Phi^{(22)}, \eta^{(22)})$:

$$R^{(22)} = 0 \tag{9a}$$

$$Q^{(22)} = \begin{cases} -X_0^{(1)}\{f(z)\Phi_{xx}^{(1)} - \dfrac{1}{h+l}\Phi_z^{(1)}\} - \Phi_x^{(21)} & \text{for } -(h-d) \le z \le 0 \\ -\Phi_x^{(21)} & \text{for } -h \le z < -(h-d) \end{cases} \tag{9b}$$

$$P^{(22)} = 0 \tag{9c}$$

and for $(\Phi, \eta) = (\Phi^{(23)}, \eta^{(23)})$:

$$R^{(23)} = 0 \tag{10a}$$

$$Q^{(23)} = f(z)\, X_{0t}^{(2)} \tag{10b}$$

$$P^{(23)} = 0. \tag{10c}$$

Here $\Phi^{(21)}$ gives the bound waves due to the interaction between first-order wave components, $\Phi^{(22)}$ describes the free waves due to the wavemaker leaving its mean position and due to $\Phi^{(21)}$ mismatching the boundary condition at the wavemaker, and $\Phi^{(23)}$ gives the free waves generated by the second-order wave board motion. If the control signal for the wavemaker is based on first-order theory alone, then the resulting second-order waves are given by $\Phi^{(2)} = \Phi^{(21)} + \Phi^{(22)}$, i.e. the spurious, free waves from $\Phi^{(22)}$ are not eliminated. Let subscript 0 (on $\Phi$ and $\eta$) denote the progressive part of a wave field then the objective for second-order wavemaker theory is to determine $X_0^{(2)}(t)$ as to produce free waves $\eta_0^{(23)}$ which eliminate these spurious, free waves $\eta_0^{(22)}$ by requiring

$$\eta_0^{(22)} + \eta_0^{(23)} = 0 \tag{11}$$

or equivalently

$$\Phi_0^{(22)} + \Phi_0^{(23)} = 0. \tag{12}$$

## 2.2. *First-order solution*

At first order it suffices to analyse a monochromatic wave in the frequency domain, since superposition and the inverse FFT can then be applied to obtain time series of paddle position for irregular waves.

The first-order solution was obtained by Biésel (1951), Ursell *et al.* (1960), Flick and Guza (1980), Sand and Donslund (1985), and others. Here the solution will be given in the compact notation provided by a complex representation.

Let the first-order paddle position for each of the wave components constituting the first-order spectrum be given by

$$X_0^{(1)} = \frac{1}{2}\left\{ - iX_a \, \mathrm{e}^{i\omega t} + \text{c.c.} \right\} \tag{13}$$

where $X_a$ is the constant complex first-order wave board amplitude at still water level and where c.c. denotes the complex conjugate of the preceding term, then the solution to the first-order problem (1) and (3) may be expressed as

$$\Phi^{(1)} = \frac{1}{2}\left\{ \frac{igX_a}{\omega} \sum_{j=0}^{\infty} c_j \frac{\cosh k_j(z+h)}{\cosh k_j h} \, \mathrm{e}^{i(\omega t - k_j x)} + \text{c.c.} \right\} \tag{14a}$$

$$\eta^{(1)} = \frac{1}{2}\left\{ X_a \sum_{j=0}^{\infty} c_j \, \mathrm{e}^{i(\omega t - k_j x)} + \text{c.c.} \right\} \tag{14b}$$

which includes both the wanted progressive-wave term and the evanescent modes which are due to the mismatch between the shape of the progressive-wave velocity profile and the shape function $f(z)$. This solution obviously satisfies the bottom boundary condition (1e), and the free surface boundary condition (1b) is easily shown to require

$$\omega^2 = gk_j \tanh k_j h. \tag{15}$$

This is the linear dispersion relation generalized to complex wave numbers, and it has

one real solution, say $k_0$, and an infinity of purely imaginary solutions ($k_1$, $k_2$, . . .), where $ik_j > 0$, $j = 1, 2, \ldots$. In order not to confuse $k_0$ with the deep water wave number we shall omit the subscript on $k$ when $j = 0$ appears explicitly (and only when it is the only index).

It may seem artificial to retain imaginary wave numbers instead of letting $k_j$, $j = 1, 2, \ldots$, be the real solutions to $-\omega^2 = gk_j \tan k_j h$. However, this choice gives a considerable reduction of the algebra involved at a later stage, and it assures the analogy between the treatment of the progressive-wave term ($j = 0$) and the evanescent modes ($j = 1, 2, \ldots$).

The coefficients $c_j$ are determined by requiring the solution to satisfy the boundary condition at the wavemaker. This is done by substituting Equations (3b) and (14a) into (1c), multiplying the equation by $\cosh k_l(z + h)$ and integrating the result over the depth. Due to the orthogonality relation

$$\int_{-h}^{0} \cosh k_j(z + h) \cosh k_l(z + h)\, dz = \begin{cases} \frac{1}{2k_j}(k_j h + \sinh k_j h \cosh k_j h) & \text{for } l = j \\ 0 & \text{for } l \neq j \end{cases} \tag{16}$$

which may readily be verified, only the term $j = l$ remains in the infinite series, and the resulting equation is solved for $c_j$ to obtain

$$c_j = \sinh k_j h \frac{\Lambda_1(k_j)}{\Lambda_2(k_j)}, \tag{17}$$

where

$$\Lambda_1(k_j) \equiv k_j \int_{-h}^{0} f(z) \cosh k_j(z + h)\, dz$$

$$= \sinh k_j h - \frac{d + l}{h + l} \sinh k_j d + \frac{1}{h + l} \frac{\cosh k_j d - \cosh k_j h}{k_j} \tag{18}$$

$$\Lambda_2(k_j) \equiv k_j \int_{-h}^{0} \cosh^2 k_j(z + h)\, dz = \frac{1}{2}(k_j h + \sinh k_j h \cosh k_j h). \tag{19}$$

In the second-order transfer functions terms asymptotically equal to $\Sigma_{j=0}^{\infty} c_j$ appear. An asymptotic method for the summation of this and other infinite series was developed by Schäffer (1993b), and it provides a reduction by orders of magnitude of the computational effort required to evaluate the transfer function that appears at second order. The method requires that leading terms of different asymptotic behaviour are separated. For this purpose the first-order transfer function is rewritten as

$$c_j = \left(\frac{\omega^2 h}{g} - \frac{h}{h + l}\right) \frac{1}{D_j(k_j)} + \frac{h}{h + l} \frac{1}{D_j(k_j)} \frac{\cosh k_j d}{\cosh k_j h} \tag{20}$$

where

$$D_j(k_j) \equiv \frac{k_j h}{2} \left(\frac{k_j h}{\sinh k_j h \cosh k_j h} + 1\right) \tag{21}$$

using that under the above assumption that either $d + l = 0$ or $d = 0$ (as necessary for convergence of the second-order solution), the sinh $k_j d$-term in Equation (18) vanishes. On the right-hand side of Equation (20) the first term behaves as $j^{-3}$ for large $j$, whereas the asymptotic behaviour of the second term is $(-1)^j j^{-3} \cos(j\pi d/h)$ independent of the frequency. The asymptotic summation method will not be derived in the present paper but reference is made to Schäffer (1993b).

For $j = 0$, Equation (17) gives the real quantity $c_0$, which is known as the Biésel transfer function in terms of which the complex amplitude $A$ of the progressive part of the first-order wavefield in Equation (14) may be related to the complex amplitude $X_a$ of the first-order paddle position through

$$A = c_0 X_a, \tag{22}$$

the elevation for the progressive part of the first-order waves being

$$\eta_0^{(1)} = \frac{1}{2}\left\{ A e^{i(\omega t - kx)} + \text{c.c.} \right\}. \tag{23}$$

With $A = a - ib$ Equations (13) and (23) may be written $X_0^{(1)} = c_0^{-1}$ ($a \sin \omega t - b \cos \omega t$) and $\eta_0^{(1)} = a \cos(\omega t - kx) + b \sin(\omega t - kx)$.

For $j = 1, 2, \ldots, c_j$ is purely imaginary.

Before we proceed to the second-order solution we shall illustrate the magnitude of the evanescent modes at the wave board. This is relevant to the importance of the interaction terms at second order and for special applications of first-order theory like active absorption relying on wave gauges mounted on the wave board. For a piston-type wavemaker, Fig. 3 compares the Biésel transfer function $c_0$ with the sum of the total evanescent mode transfer function $i\Sigma_{j=1}^{\infty} c_j$ for (a) a piston-type wavemaker, (b) a bottom-hinged wavemaker, and (c) a hinged-type wavemaker where the hinge is placed halfway from the surface to the bottom. While $c_0$ has the asymptotic value of 2 (which in case of a piston-type wavemaker is practically reached at the traditional deep water limit) the total evanescent mode transfer function increases continuously with increasing dimensionless frequency or depth. It appears that for the piston-type wavemaker the amplitude of the evanescent modes at the wave board exceeds the amplitude of the emitted progressive wave when $2\pi f \sqrt{h/g} > 3.35$, corresponding to $kh > 11.2$. This demonstrates the problems of generating deep water waves with a piston-type wavemaker, since pronounced evanescent modes will contribute significantly to the nonlinear wave interaction. When the distance to the centre of rotation is finite, then the wave board motion has its best fit to the velocity profile of the progressive wave for a dimensionless frequency $2\pi f \sqrt{h/g} > 0$, as also indicated by the zeros of $i\Sigma_{j=1}^{\infty} c_j$ in Fig. 3(b) and (c).

### 2.3. *Second-order solution*

At second order, interactions between two wave components of generally different angular frequencies $\omega_n$ and $\omega_m$ constitute the basis of the second-order spectrum. The interaction terms appear as subharmonics (difference frequencies) and superharmonics (sum frequencies) and thus bichromatic waves should be analysed in the frequency domain and superposition and the inverse FFT can then be applied to obtain second-

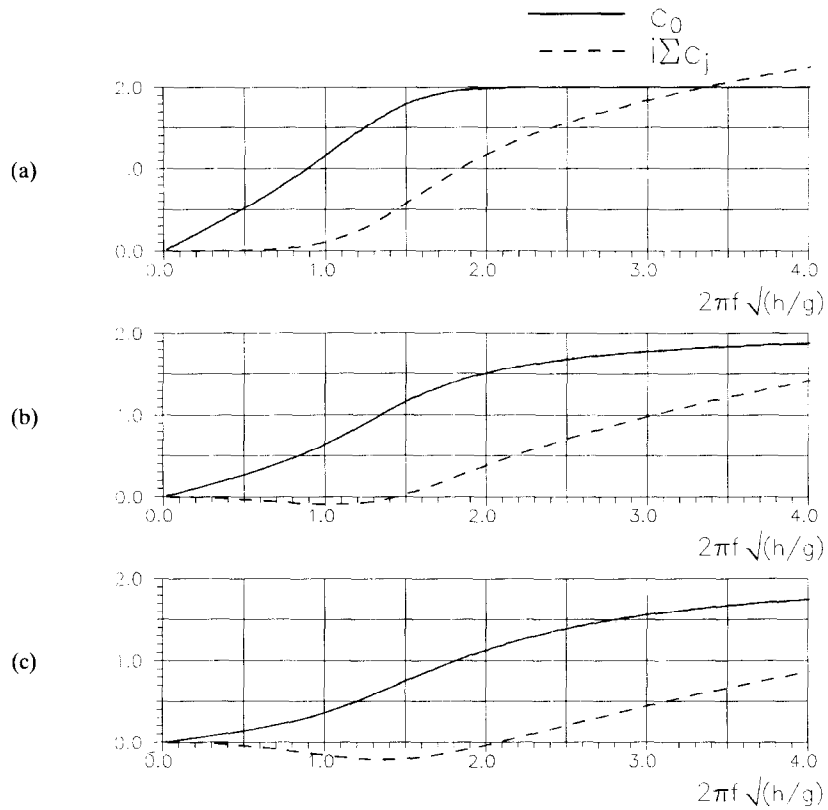


Fig. 3. The Biésel transfer function $c_0$ and the total evanescent mode transfer function $i\Sigma_{j=0}^{\infty} c_j$ for (a) a piston-type wavemaker ($l = \infty$), (b) a bottom-hinged wavemaker ($d = l = 0$), and (c) a hinged-type wave maker where the hinge is placed halfway from the surface to the bottom ($d = -l = h/2$).

order time series of paddle position for irregular waves to be added to the corresponding first-order time series.

The aim of second-order wave generation is to get a second-order bound surface elevation $\eta_0^{(21)\pm}$ without any spurious free-wave generation.

The summation indices for the series (14) giving the first-order solution for $\omega_n$ and $\omega_m$ are denoted $j$ and $l$, respectively, and if $S^{(21)}$ stands for each of the quantities $R^{(21)}$, $\Phi^{(21)}$, $P^{(21)}$, and $\eta^{(21)}$, then $S_{jnlm}^{(21)+}$ and $S_{jnlm}^{(21)-}$ denote the complex superharmonic and subharmonic contributions, respectively, for the interaction between each pair of terms drawn from the two series, i.e.

$$S^{(21)} = \frac{1}{2}\left\{\sum_{j=0}^{\infty}\sum_{l=0}^{\infty}\left[S_{jnlm}^{(21)+} + S_{jnlm}^{(21)-}\right] + \text{c.c.}\right\}; S^{(21)} = \begin{cases} R^{(21)} \\ \Phi^{(21)} \\ P^{(21)} \\ \eta^{(21)} \end{cases} \tag{24}$$

Using Equation (15) to eliminate any appearing $\tanh k_j h$-term, Equations (8a) and (14) yield, after straightforward but lengthy algebra,

$$R^{(21)\pm}_{jnlm} = \delta_{nm}\left\{iX_n X_m^{-:*} c_{jn} c_{lm}^{-:*} e^{i(\theta_{jn}\pm\theta_{lm}^{-:*})}\right.$$
$$\left.\left[\omega_n \omega_m^2 \mp \frac{g^2 k_{jn} k_{lm}^{-:*}}{\omega_n} \pm \frac{1}{2}\left(\omega_m^3 - \frac{g^2 k_{lm}^2}{\omega_m}\right)\right] \pm \widehat{lmjn}^{-:*}\right\} \tag{25a}$$
$$= \delta_{nm} H^{\pm}_{jnlm}\, iX_n X_m^{-:*} c_{jn} c_{lm}^{-:*} e^{i(\theta_{jn}\pm\theta_{lm}^{-:*})},$$

where

$$\delta_{nm} \equiv \begin{cases} \frac{1}{2} & \text{for } n = m \\ 1 & \text{for } n \neq m \end{cases} \tag{25b}$$

$$\theta_{jn} \equiv \omega_n t - k_{jn} x; \qquad \theta_{lm} \equiv \omega_m t - k_{lm} x \tag{25c}$$

and $\widehat{lmjn}$ means "the preceding term permuting $l$ and $j$ as well as $m$ and $n$". This symbol is used throughout even in cases where $l$ or $j$ are explicitly given as zero. Furthermore,

$$H^{\pm}_{jnlm} \equiv (\omega_n \pm \omega_m)\left(\pm\omega_n\omega_m - \frac{g^2 k_{jn} k_{lm}^{-:*}}{\omega_n\omega_m}\right) + \frac{\omega_n^3 \pm \omega_m^3}{2} - \frac{g^2}{2}\left(\frac{k_{jn}^2}{\omega_n} \pm \frac{k_{lm}^2}{\omega_m}\right) \tag{25d}$$

and the symbol $^{-:*}$ introduced for brevity is defined by

$$Z^{-:*} = \begin{cases} Z & \text{for superharmonics} \\ Z^* & \text{for subharmonics,} \end{cases} \tag{26}$$

where * denotes complex conjugation, i.e. $^{-:*}$ is to be interpreted as complex conjugation in case of subharmonics, while being ignored for superharmonics. Furthermore, the complex identity

$$\{Z_1 e^{iz_1} + \text{c.c.}\}\{Z_2 e^{iz_2} + \text{c.c.}\} = \left\{Z_1 Z_2 e^{i(z_1+z_2)} + Z_1 Z_2^* e^{i(z_1-z_2^*)}\right\} + \text{c.c.}, \tag{27}$$

where $z_1$, $z_2$, $Z_1$, $Z_2$ are complex numbers, has been used. This identity reveals the origin of the distinction (26) between the superharmonics and the subharmonics used in Equation (25). (Note that originally the term $\pm\widehat{lmjn}^{-:*}$ in Equation (25a) would appear outside the braces and without the conjugation symbol. However, it is seen that Equation (24) still holds irrespective of whether or not the complex conjugation is imposed on a term in $R^{(21)\pm}_{jnlm}$, and accordingly $\widehat{lmjn}^{-:*}$ may well be used instead of $\widehat{lmjn}$. Due to the factor $i$, $lmjn^{-:*}$ becomes $\pm lmjn^{-:*}$ when moved inside the braces.)

It follows that the solution to Equations (1a,b,e) and (8a) is†

† In most of the previous papers on the subject involving more than one primary frequency, only the contribution from the progressive first-order waves, i.e. $(j,l) = (0,0)$ has been considered. It appears that all contributions $(j,l)$ enter the transfer functions used for second-order wave generation.

$$\Phi_{jnlm}^{(21)\pm} = \frac{R_{jnlm}^{(21)\pm}}{D_{jnlm}^{\pm}} \frac{\cosh(k_{jn} \pm k_{lm}^{-:*})(z+h)}{\cosh(k_{jn} \pm k_{lm}^{-:*})h} \tag{28a}$$

where

$$D_{jnlm}^{\pm} \equiv g(k_{jn} \pm k_{lm}^{-:*}) \tanh(k_{jn} \pm k_{lm}^{-:*})h - (\omega_n \pm \omega_m)^2. \tag{28b}$$

For $(j,l) = (0,0)$ Equation (28) is real and it is consistent with Dean and Sharma (1981).

We now turn to the corresponding surface elevation. From Equations (8c) and (14) we obtain

$$\begin{aligned} P_{jnlm}^{(21)\pm} &= \delta_{nm}\left\{X_n X_m^{-:*} c_{jn} c_{lm}^{-:*} e^{i(\theta_{jn} \pm \theta_{lm}^{-:*})}\right. \\ &\quad \left.\left[\frac{g^2 k_{jn} k_{lm}^{-:*}}{4\omega_n\omega_m} \mp \frac{1}{4}\omega_n\omega_m - \frac{1}{2}\omega_m^2\right] + \widehat{lmjn}^{-:*}\right\} \qquad (29a) \\ &= \delta_{nm} L_{jnlm}^{\pm} X_n X_m^{-:*} c_{jn} c_{lm}^{-:*} e^{i(\theta_{jn} \pm \theta_{lm}^{-:*})} \end{aligned}$$

where

$$L_{jnlm}^{\pm} \equiv \frac{1}{2}\left\{\frac{g^2 k_{jn} k_{lm}^{-:*}}{\omega_n\omega_m} \mp \omega_n\omega_m - (\omega_n^2 + \omega_m^2)\right\} \tag{29b}$$

which by Equation (1d) yields

$$\eta_{jnlm}^{(21)\pm} = G_{jnlm}^{\pm} X_n X_m^{-:*} c_{jn} c_{lm}^{-:*} e^{i(\pm_{jn} \pm \theta_{lm}^{-:*})} \tag{30a}$$

where

$$G_{jnlm}^{\pm} \equiv \frac{\delta_{nm}}{g}\left\{(\omega_n \pm \omega_m)\frac{H_{jnlm}^{\pm}}{D_{jnlm}^{\pm}} - L_{jnlm}^{\pm}\right\}. \tag{30b}$$

For $(j,l) = (0,0)$ this gives the progressive part of the second-order bound wave, and $G_{0n0m}^{\pm}$ can be shown to equal the transfer functions $G_{nm}^{\pm}$ given by Ottesen-Hansen (1978) and Sand and Mansard (1986a,b), and we have†

† In the papers by Sand (1982), Barthel *et al.* (1983) and Sand and Donslund (1985), the transfer function $G_{nm}^{-}$ for the second-order surface elevation as found by Ottesen-Hansen (1978) was used in connection with $\Phi^{(21)-}$ as if $\eta^{(21)-}$ was a free wave, i.e. Equation (1d) was solved for $\Phi^{21-}$ neglecting that $p^{(21)-} \neq 0$, cf. Equation (8c). In terms of the quantities defined above, the term $L_{0n0m}^{-}$ ($L_{nm}^{-}$ for short) was retained in the transfer function for $\Phi^{(21)-}$. This was corrected for the superharmonics, cf. Sand and Mansard (1986a,b) and Mansard *et al.* (1987) by introducing a so-called $U^{\pm}$-factor, which may be shown to satisfy

$$U^{\pm} = \frac{g(k_n \pm k_m)\tanh(k_n \pm k_m)h}{(\omega_n \pm \omega_m)^2} \frac{G_{nm}^{\pm} + \delta_{nm} L_{nm}^{\pm}/g}{G_{nm}^{\pm}}.$$

In the present formulation $H_{jnlm}^{\pm}/D_{jnlm}^{\pm}$ is used directly in the transfer function $\mathcal{F}^{\pm}$ in Equation (37) relating the second-order wavemaker control signal to the primary wave amplitudes without using the more complicated $G_{nm}^{\pm}$ and $U^{\pm}$-factors.

$$\eta_0^{(21)\pm} = \frac{1}{2}\left\{G_{nm}^{\pm} A_n A_m^{-:*} e^{i(\theta_{0n} \pm \theta_{0m})} + \text{c.c.}\right\}. \tag{31a}$$

With $A_n = a_n - ib_n$ and $A_m^{-:*} = a_m \mp ib_m$, Equation (31a) may be written

$$\eta_0^{(21)\pm} = G_{nm}^{\pm}\{(a_n a_m \mp b_n n_m)\cos(\theta_{0n} \pm \theta_{0m}) + (\pm a_n b_m + a_m b_n)\sin(\theta_{0n} \pm \theta_{0m})\}. \tag{31b}$$

It should be emphasized that in the present formulation of second-order wavemaker theory the above calculations of $\eta^{(21)}$ and $G^{\pm}_{jnlm}$ are not needed.

$G^{-}_{nm}h/\delta_{nm}$ and $G^{+}_{nm}h/\delta_{nm}$ are shown in Fig. 4. Notice, that if one of the two frequencies corresponds to a shallow water wave, then the subharmonic and the superharmonic transfer functions are of equal magnitude and opposite sign.

The remaining contributions at second order, $\Phi^{(22)}$ and $\Phi^{(23)}$, represent free waves, and the analogy to the first-order solution is evident, since the function $Q$, cf. Equations (3b), (9b), (10b), gives the only deviation from the first-order problem. Thus, following the same procedure as for the first-order waves only, now for superharmonic and subharmonic frequencies, we have

$$\Phi^{(22)} = \Phi^{(22)+} + \Phi^{(22)-} \tag{32a}$$

$$\eta^{(22)} = \eta^{(22)+} + \eta^{(22)-} \tag{32b}$$

$$\Phi^{(22)\pm} = \frac{1}{2}\left\{\frac{igA_n A_m^{-:*}}{h(\omega_n \pm \omega_m)} \sum_{p=0}^{\infty} c_p^{(22)\pm} \frac{\cosh K_p^{\pm}(z+h)}{\cosh K_p^{\pm} h} e^{i((\omega_n \pm \omega_m)t - K_p^{\pm} x)} + \text{c.c.}\right\} \tag{32c}$$

$$\eta^{(22)\pm} = \frac{1}{2}\left\{\frac{A_n A_m^{-:*}}{h} \sum_{p=0}^{\infty} c_p^{(22)\pm} e^{i((\omega_n \pm \omega_m)t - K_p^{\pm} x)} + \text{c.c.}\right\} \tag{32d}$$

which includes the progressive-wave term as well as the evanescent modes. Here $K_p^{\pm}$ is the solution to

$$(\omega_n \pm \omega_m)^2 = gK_p^{\pm} \tanh K_p^{\pm} h \tag{33}$$

which is the linear dispersion relation generalized to complex wave numbers, cf. Equation (15) and the discussion there. Using Equations (32c) and (9b) in (1c) and multiplying the resulting equation by $\cosh K_l^{\pm}(z+h)$, integration from $z = -h$ to $z = 0$ gives the coefficients $c_p^{(22)\pm}$ by virtue of orthogonality, exactly as in the first-order case. We get

$$c_p^{(22)\pm} = \delta_{nm} \frac{h(\omega_n \pm \omega_m)\cosh K_p^{\pm} h}{gc_{0n}c_{0m}\Lambda_2(K_p^{\pm})}\left\{\pm \frac{g}{2\omega_n} \sum_{j=0}^{\infty} \frac{c_{jn}k_{jn}}{\cosh k_{jn}h} \Gamma_4(k_{jn}, K_p^{\pm}) + \widehat{lmjn}^{-:*} - \sum_{j=0}^{\infty}\sum_{l=0}^{\infty} c_{jn}\, c_{lm}^{-:*} \frac{k_{jn} \pm k_{lm}^{-:*}}{\cosh(k_{jn} \pm k_{lm}^{-:*})h} \frac{H_{jnlm}^{\pm}}{D_{jnlm}^{\pm}} \Gamma_1(k_{jn} + k_{lm}^{-:*}, K_p^{\pm})\right\} \tag{34}$$

Fig. 4. (opposite) Second-order superharmonic and subharmonic transfer functions $G_{nm}h^{+}$ vs dimensionless first-order frequencies $2\pi f_n\sqrt{h/g}$ and $2\pi f_m\sqrt{h/g}$. Contour lines are a subset of $(0, \pm 1/n, n = 1, 2, \ldots, 10\ldots)$.

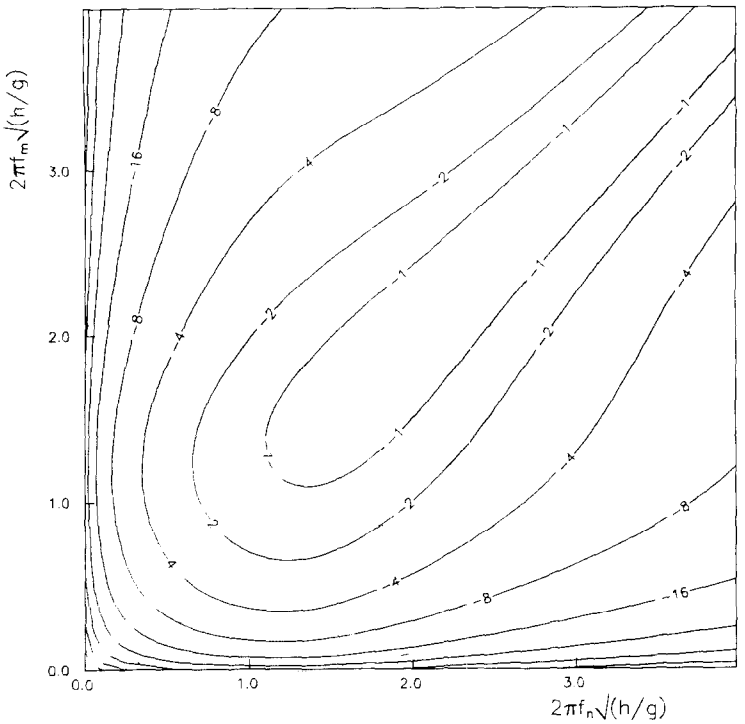
$2\pi f_m\sqrt{(h/g)}$
3.0
2.0
1.0
0.0
0.0
1.0
2.0
3.0
$2\pi f_n\sqrt{(h/g)}$

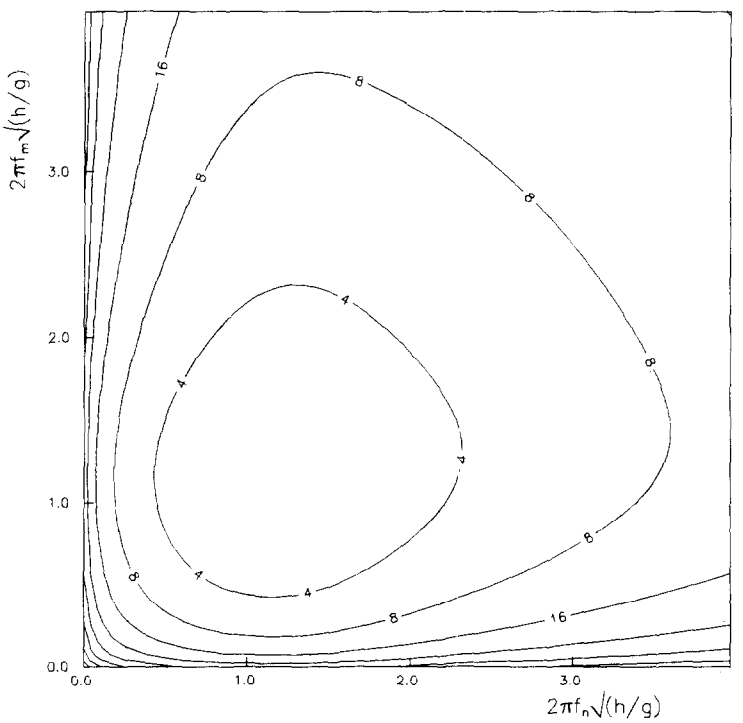
$2\pi f_m\sqrt{(h/g)}$
3.0
2.0
1.0
0.0
0.0
1.0
2.0
3.0
$2\pi f_n\sqrt{(h/g)}$

where

$$\Gamma_1(\kappa_1, \kappa_2) \equiv \int_{-h}^{0} \cosh \kappa_1(z+h) \cosh \kappa_2(z+h)\, dz \tag{35a}$$

and

$$\Gamma_4(\kappa_1, \kappa_2) \equiv \kappa_1 \Gamma_2(\kappa_1, \kappa_2) + \frac{1}{h+l} \Gamma_3(\kappa_1, \kappa_2) \tag{35b}$$

where

$$\Gamma_2(\kappa_1, \kappa_2) \equiv \int_{-h+d}^{0} f(z) \cosh \kappa_1(z+h) \cosh \kappa_2(z+h)\, dz \tag{35c}$$

and†

$$\Gamma_3(\kappa_1, \kappa_2) \equiv \int_{-h+d}^{0} \sinh \kappa_1(z+h) \cosh \kappa_2(z+h)\, dz. \tag{35d}$$

The functions $\Gamma_{1\ldots4}$ are evaluated in the Appendix. Using $\Gamma_1\ (k_{jn} \pm k_{lm}^{-:*},\ K_p^{\pm})$ and $\Gamma_4\ (k_{jn},\ K_p^{\pm})$ as given in Equations (A9) and (A10), Equation (34) reduces to‡

$$c_p^{(22)\pm} = \delta_{nm} \frac{h(\omega_n \pm \omega_m) \cosh^2 K_p^{\pm} h}{g^2 c_{0n} c_{0m} \Lambda_2 K_p^{\pm}} \left\{ \pm \frac{g}{2\omega_n} \sum_{j=0}^{\infty} \frac{c_{jn} k_{jn}^2}{k_{jn}^2 - (K_p^{\pm})^2} \left( \omega_n^2 - (\omega_n \pm \omega_m)^2 + M_2(k_{jn}, K_p^{\pm}) \right) + \widehat{lmjn}^{-:*} - \sum_{j=0}^{\infty} \sum_{l=0}^{\infty} c_{jn}\, c_{lm}^{-:*} \frac{k_{jn} \pm k_{lm}^{-:*}}{(k_{jn} \pm k_{lm}^{-:*})^2 - (K_p^{\pm})^2} H_{jnlm}^{\pm} \right\} \tag{36a}$$

where

$$M_2(k_{jn}, K_p^{\pm}) \equiv -\frac{g}{h+l} \frac{K_p^{\pm}/k_{jn}}{k_{jn}^2 - (K_p^{\pm})^2} \left\{ 2k_{jn} K_p^{\pm} \left( 1 - \frac{\cosh k_{jn} d \cosh K_p^{\pm} d}{\cosh k_{jn} h \cosh K_p^{\pm} h} \right) - (k_{jn}^2 + (K_p^{\pm})^2) \left( \frac{\omega_n^2 (\omega_n \pm \omega_m)^2}{g^2 k_{jn} K_p^{\pm}} - \frac{\sinh k_{jn} d \sinh K_p^{\pm} d}{\cosh k_{jn} h \cosh K_p^{\pm} h} \right) \right\} \tag{36b}$$

vanishes for a piston-type wavemaker.

The denominator $D_{jnlm}^{\pm}$ and thereby one explicit shallow water singularity have now vanished from the expression.

We now turn to $\Phi^{(23)}$. Let the second-order paddle position be given by

$$X_0^{(2)\pm} = \frac{1}{2} \left\{ -i\mathcal{F}^{\pm} \frac{A_n A_m^{-:*}}{h} e^{i(\omega_n \pm \omega_m)t} + \text{c.c.} \right\} \tag{37}$$

† Here lower bound of the integral for $\Gamma_3$ must be taken as $-h + d$ (instead of just $-h$), cf. Equation (9b) and the footnote in connection with Equation (4b). In the integral for $\Gamma_2$, however, either lower bound may be used since $f(z) \equiv 0$ for $-h \le z < -h + d$.

‡ For $p = j = 0$ and $\omega_m = 2\omega_n$ there is a removable singularity in the single summation in case of subharmonics, cf. Equations (A8) and (A10) in the appendix. (If $\omega_m < \omega_n$ is chosen then this appears for $p = j = 0$ and $2\omega_m = \omega_n$ in the series implicitly contained in the $\widehat{lmjn}^{-:*}$-term).

and let

$$\Phi^{(23)} = \Phi^{(23)+} + \Phi^{(23)-} \tag{38a}$$

$$\eta^{(23)} = \eta^{(23)+} + \eta^{(23)-} \tag{38b}$$

then

$$\Phi^{(23)\pm} = \frac{1}{2}\left\{\frac{ig\mathcal{F}^{\pm} A_n A_m^{-:*}}{h(\omega_n \pm \omega_m)} \sum_{p=0}^{\infty} c_p^{(23)\pm} \frac{\cosh K_p^{\pm}(z+h)}{\cosh K_p^{\pm} h} e^{i((\omega_n \pm \omega_m)t - K_p^{\pm}x)} + \text{c.c.}\right\} \tag{38c}$$

$$\eta^{(23)\pm} = \frac{1}{2}\left\{\mathcal{F}^{\pm} \frac{A_n A_m^{-:*}}{h} \sum_{p=0}^{\infty} c_p^{(23)\pm} e^{i((\omega_n \pm \omega_m)t - K_p^{\pm}x)} + \text{c.c.}\right\} \tag{38d}$$

where

$$c_p^{(23)\pm} = \sinh K_p^{\pm} h \frac{\Lambda_1(K_p^{\pm})}{\Lambda_2(K_p^{\pm})}, \tag{39}$$

cf. Equation (17). From Equation (11) or (12) we obtain the transfer function

$$\mathcal{F}^{\pm} = -\frac{c_0^{(22)\pm}}{c_0^{(23)\pm}}. \tag{40}$$

Note that this only assures that the progressive-wave terms ($p = 0$) in Equations (32) and (38) cancel, i.e. the evanescent modes ($p = 1, 2, \ldots$) may still remain. From Equations (36) and (39), we further get [see footnote to Equation (36)]

$$\mathcal{F}^{\pm} = E^{\pm}\left\{\mp \frac{g}{2\omega_n} \sum_{j=0}^{\infty} c_{jn} \frac{k_{jn}^2}{k_{jn}^2 - (K_0^{\pm})^2}\left(\omega_n^2 - (\omega_n \pm \omega_m)^2 + M_2(k_{jn}, K_0^{\pm})\right) + \widehat{lmjn}^{-:*}\right.$$

$$\left. + \sum_{j=0}^{\infty}\sum_{l=0}^{\infty} c_{jn} c_{lm}^{-:*} \frac{k_{jn} \pm k_{lm}^{-:*}}{(k_{jn} \pm k_{lm}^{-:*})^2 - (K_0^{\pm})^2} H_{jnlm}^{\pm}\right\} \tag{41a}$$

where

$$E^{\pm} \equiv \frac{\delta_{nm}(K_0^{\pm})^2 h}{c_{0n} c_{0m}(\omega_n \pm \omega_m)^3 (1 + M_1(K_0^{\pm}))} \tag{41b}$$

and

$$M_1(K_0^{\pm}) \equiv \frac{1}{h + l(\omega_n \pm \omega_m)^2}\frac{g}{}\left(\frac{\cosh K_0^{\pm} d}{\cosh K_0^{+} h} - 1\right) \tag{41c}$$

vanishes for a piston-type wavemaker. This is the main result of the theory.

Be warned that, except for shallow water conditions, straightforward summation of the double infinite series in Equation (41a) requires a great number of terms before a reasonable accuracy is obtained. For regular waves and wave groups this is not a problem with modern computers, but it does become a formidable task in the case where a whole spectrum of primary waves needs to be resolved. For this reason an asymptotic summation method was developed (see Schäffer, 1993b), providing a reduction by orders of magnitude of the computational effort required to evaluate $\mathcal{F}^{\pm}$.

An example of the method is given in Fig. 5, which shows the estimate of an infinite sum using the asymptotic summation method as well as straightforward summation vs the maximum summation index $J$ up to $J = 50$, with the correct value of the infinite sum based on $J = 500$ given for reference. The examples are from the real part of the inner series in the double infinite sum in Equation (41a), which is typical for the series constituting the double infinite sum. No direct comparison with the magnitude of $\mathcal{F}^{\pm}$ can be made from the figures, since a factor was omitted in the examples given. The results are shown for two different wavemakers for the superharmonic with dimen-

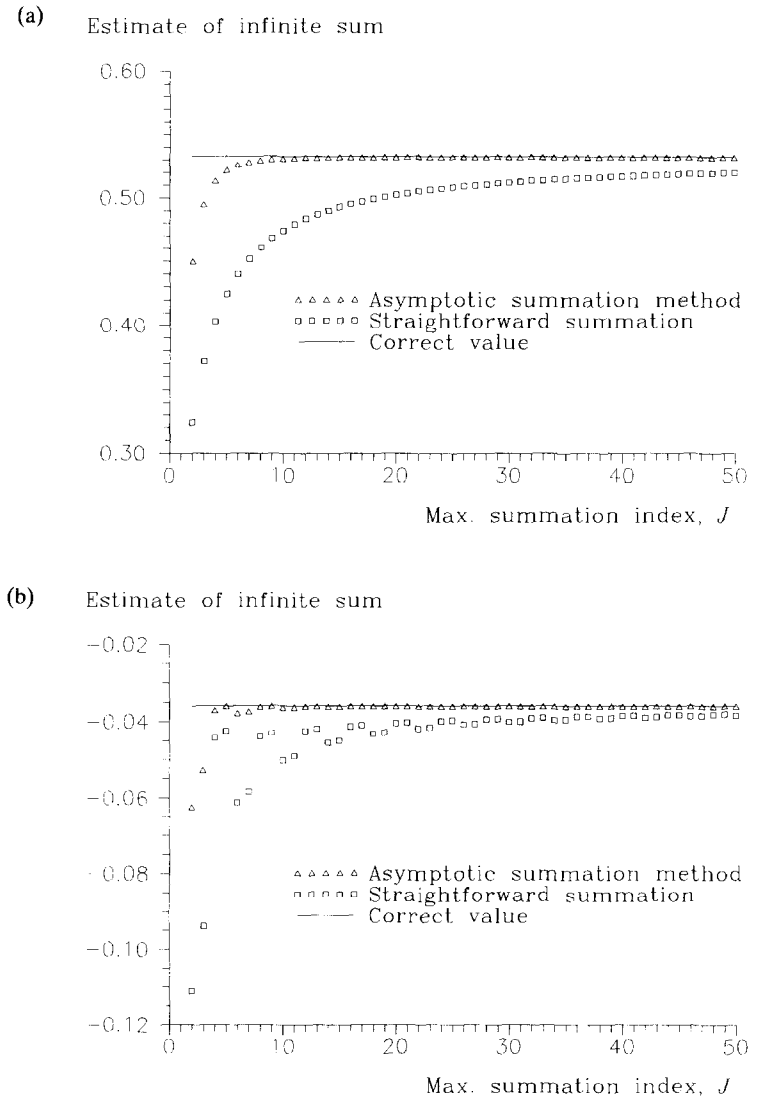


Fig. 5. Typical examples of the capability of the asymptotic summation method for part of the superharmonic second-order transfer function for (a) a piston-type wavemaker, (b) a hinged-type wavemaker where the hinge is placed halfway from the surface to the bottom.

sionless first-order frequencies $2\pi f_n\sqrt{h/g} = 2\pi f_m\sqrt{h/g} = 1.5$. In Fig. 5(a) a piston-type wavemaker is considered while Fig. 5(b) gives results for the hinged type where the hinge is located halfway from the surface to the bottom.

In the example of Fig. 5(a) a maximum error of 1% requires $J = 6$ when using the asymptotic summation method, while straightforward summation requires no less than $J = 115$. If the maximum error accepted is relaxed to 3%, then the numbers are $J = 4$ and $J = 32$, respectively. Generally the advantage of the asymptotic method is larger if higher accuracy is required, but typically a reduction in the computational effort of a factor 10 is obtained. Since this applies for both index $l$ and index $j$ in the double infinite series, the resulting reduction is of the order of a factor 100.

Sand (1982), Barthel *et al.* (1983), Sand and Donslund (1985) and Sand and Mansard (1986a,b) used three transfer functions denoted $F_{11}$, $F_{12}$, and $F_{23}$. These functions all eliminate free waves which otherwise would have been emitted from the wave paddle due to the interaction between the following combinations of two first-order terms [the terms referenced are in Equation (41)]:

(i) progressive-wave component and progressive-wave component ($F_{11}$ or the first term in the double summation, $j = l = 0$);
(ii) component of paddle position and progressive-wave component ($F_{12}$ or the first term in the single summation, $j = 0$);
(iii) component of paddle position and evanescent-mode component ($F_{23}$ or the rest of the single summation, $j = 1, 2, \ldots$).

Schaeffer considera os modos evan.

In addition to these terms Equation (41) comprises two qualitatively different terms both related to the first-order evanescent modes. These terms are present in order to eliminate the emission of free waves due to the interaction between the first-order terms:

Acho eu Sand não considera

(iv) progressive-wave component and evanescent-mode component ($F_{13}$ and $F_{24}$ defined below or $j = 0$, $l = 1, 2, \ldots$ and vice versa in the double summation);
(v) evanescent mode component and evanescent mode component ($F_{22}$ defined below or the rest of the double summation, $j = 1, 2, \ldots$, $l = j = 1, 2, \ldots$).

Except for the corrections given previously as footnotes, the function $\mathcal{F}^{\pm}$ (excluding the new terms) is consistent with the findings in the above-referenced papers.

The terms mentioned under (iv) and (v) are included in the analysis for regular waves given by Fontanet (1961), Hudspeth and Sulisz (1991), Sulisz and Hudspeth (1993), and for the bichromatic extension of Moubayed and Williams (1994) and also recognized although not included by Suh and Dalrymple (1987).

With $A_n = a_n - ib_n$ and $A_m^{-*} = a_m \mp ib_m$ we have in a real representation

$$X_0^{(2)\pm} = \frac{\mathcal{R}\{\mathcal{F}^{\pm}\}}{h}\{(a_n a_m \mp b_n b_m)\sin(\omega_n \pm \omega_m)t + (\mp a_n b_m - a_m b_n)\cos(\omega_n \pm \omega_m)t\}$$

$$- \frac{\mathcal{I}\{\mathcal{F}^{\pm}\}}{h}\{(\mp a_n b_m - a_m b_n)\sin(\omega_n \pm \omega_m)t - (a_n a_m \mp b_n b_m)\cos(\omega_n \pm \omega_m)t\}. \quad (42)$$

The new term (iv) mentioned above makes it tedious to derive the real and imaginary parts of the transfer function (41), since the complex term $k_{jn} \pm k_{lm}^{-*}$ in this case is

neither real nor purely imaginary. It is recommended to use the relatively simple complex formulation for practical application and to let a computer separate the complex result whenever appropriate in the actual implementation. However, we shall derive $\mathcal{R}\{\mathcal{F}^{\pm}\}$ and $\mathcal{I}\{\mathcal{F}^{\pm}\}$ for the sake of comparison with $F_{11}$, $F_{12}$ and $F_{23}$.

$\mathcal{R}\{\mathcal{F}^{\pm}\}$ and $\mathcal{I}\{\mathcal{F}^{\pm}\}$ may be split up into three contributions:

$$\mathcal{R}\{\mathcal{F}^{\pm}\} = \mp (F_{11}^{\pm} + F_{12}^{\pm} + F_{13}^{\pm})\, h \tag{43}$$

and

$$\mathcal{I}\{\mathcal{F}^{\pm}\} = (F_{22}^{\pm} + F_{23}^{\pm} + F_{24}^{\pm})\, h \tag{44}$$

where the factor $h$ is included for historical reasons.

In addition to the well-known transfer functions $F_{11}^{\pm}$, $F_{12}^{\pm}$ and $F_{23}^{\pm}$ three new functions $F_{13}^{\pm}$, $F_{22}^{\pm}$ and $F_{24}^{\pm}$ appear. (The succession of indices as well as the sign convention has been chosen to match the definitions of the old functions $F_{11}^{\pm}$, $F_{12}^{\pm}$ and $F_{23}^{\pm}$.) Remembering that $c_{jn}$ ($c_{lm}$) and $k_{jn}$ ($k_{lm}$) are real for $j = 0$ ($l = 0$) and purely imaginary for $j = 1, 2, \ldots$ ($l = 1, 2, \ldots$), we get†

$$F_{11}^{\pm} h = E^{\pm} \frac{k_{0n} \pm k_{0m}}{(k_{0n} \pm k_{0m})^2 - (K_0^{\pm})^2} H_{0n0m}^{\pm} \tag{45}$$

$$F_{12}^{\pm} h = \mp E^{\pm} \left\{ \frac{g}{2\omega_n} c_{0n} \frac{k_{0n}^2}{k_{0n}^2 - (K_0^{\pm})^2} \left( \omega_n^2 - (\omega_n \pm \omega_m)^2 + M_2(k_{0n}, K_0^{\pm}) \right) + \widehat{0m0n} \right\} \tag{46}$$

$$F_{13}^{\pm} h = E^{\pm} \sum_{j=1}^{\infty} \frac{c_{jn} c_{0m}}{(k_{jn}^2 + k_{0m}^2 - (K_0^{\pm})^2)^2 - 4k_{jn}^2 k_{0m}^2} \left\{ k_{jn} (k_{jn}^2 - k_{0m}^2 - (K_0^{\pm})^2)\, \mathcal{R}\{H_{jn0m}\} \pm k_{0m} (-k_{jn}^2 + k_{0m}^2 - (K_0^{\pm})^2)\, i\mathcal{I}\{H_{jn0m}\} \right\} + \widehat{lm0n} \tag{47}$$

and

$$iF_{22}^{\pm} h = E^{\pm} \sum_{j=1}^{\infty} \sum_{l=1}^{\infty} c_{jn}\, c_{lm}^{-:*} \frac{k_{jn} \pm k_{lm}^{-:*}}{(k_{jn} \pm k_{lm}^{-:*})^2 - (K_0^{\pm})^2} H_{jnlm}^{\pm} \tag{48}$$

$$iF_{23}^{\pm} h = \mp E^{\pm} \left\{ \frac{g}{2\omega_n} \sum_{j=1}^{\infty} c_{jn} \frac{k_{jn}^2}{k_{jn}^2 - (K_0^{\pm})^2} (\omega_n^2 - (\omega_n \pm \omega_m)^2 + M_2(k_{jn}, K_0^{\pm})) \pm \widehat{lmjn} \right\} \tag{49}$$

† For $F_{12}^{-}$, see the footnote to Equation (36).

$$iF_{24}^{\pm}h = E^{\pm}\sum_{j=1}^{\infty}\frac{c_{jn}c_{0m}}{(k_{jn}^2+k_{0m}^2-(K_0^{\pm})^2)^2-4k_{jn}^2k_{0m}^2}\Big\{k_{jn}(k_{jn}^2-k_{0m}^2-(K_0^{\pm})^2)\,i\mathcal{I}\{H_{jn0m}\}$$
$$\pm k_{0m}(-k_{jn}^2+k_{0m}^2-(K_0^{\pm})^2)\,\mathcal{R}\{H_{jn0m}\}\Big\}$$
$$\pm \widehat{lm0n} \tag{50}$$

where from Equation (25d)

$$\mathcal{R}\{H_{jn0m}\} = \pm(\omega_n \pm \omega_m)\,\omega_n\omega_m + \frac{\omega_n^3 \pm \omega_m^3}{2} - \frac{g^2}{2}\left(\frac{k_{jn}^2}{\omega_n} \pm \frac{k_{0m}^2}{\omega_m}\right) \tag{51a}$$

$$i\mathcal{I}\{H_{jn0m}\} = -(\omega_n \pm \omega_m)\frac{g^2\,k_{jn}k_{0m}}{\omega_n\omega_m}. \tag{51b}$$

For the same three wavemaker configurations as in Fig. 3, Fig. 6 shows the real and imaginary parts of the subharmonic complex transfer function $\mathcal{F}^-/\delta_{nm}$ vs dimensionless first-order frequencies $2\pi f_n\sqrt{h/g}$ and $2\pi f_m\sqrt{h/g}$. Figure 7(a) and (b) shows the equivalent for the superharmonics.

Previously it was generally acknowledged that the interaction terms involving the evanescent modes were insignificant for the subharmonics, whereas they had to be included when superharmonics were to be generated correct to second order.

This has led some laboratories primarily interested in the subharmonics to neglect the evanescent mode interactions, since these are much more complicated to incorporate. The new interaction terms do, however, change the results of the theory significantly and the question is whether the conclusion regarding their importance still holds. In Schäffer (1994) the error made by disregarding the influence of the evanescent modes in second-order regular and irregular wave generation was quantified. The conclusion of this analysis was that neglecting the evanescent mode contributions results in substantial errors for subharmonics as well as for superharmonics unless the waves are generated by a piston-type wavemaker in the intermediate to shallow water range.

## 3. RANGE OF APPLICABILITY

It is well known that Stokes second-order theory becomes invalid in shallow water, where it predicts too large second-order components even for very moderate wave steepnesses. For regular waves the theory has traditionally been rejected when it predicted secondary peaks appearing in the trough of the primary wave. The limiting case corresponds to a superharmonic amplitude of one-fourth of the primary wave amplitude. Introducing a parameter $S$ given by

$$S = 2H\left|G_{nm}^{\pm}\right| \tag{52}$$

as a measure of nonlinearity, this corresponds to $S = 1$, see Equations (23) and (31). For wave groups and irregular waves Equation (52) can still be used as an indication of how well the theory performs taking $H$ to be a characteristic wave height.

(a)

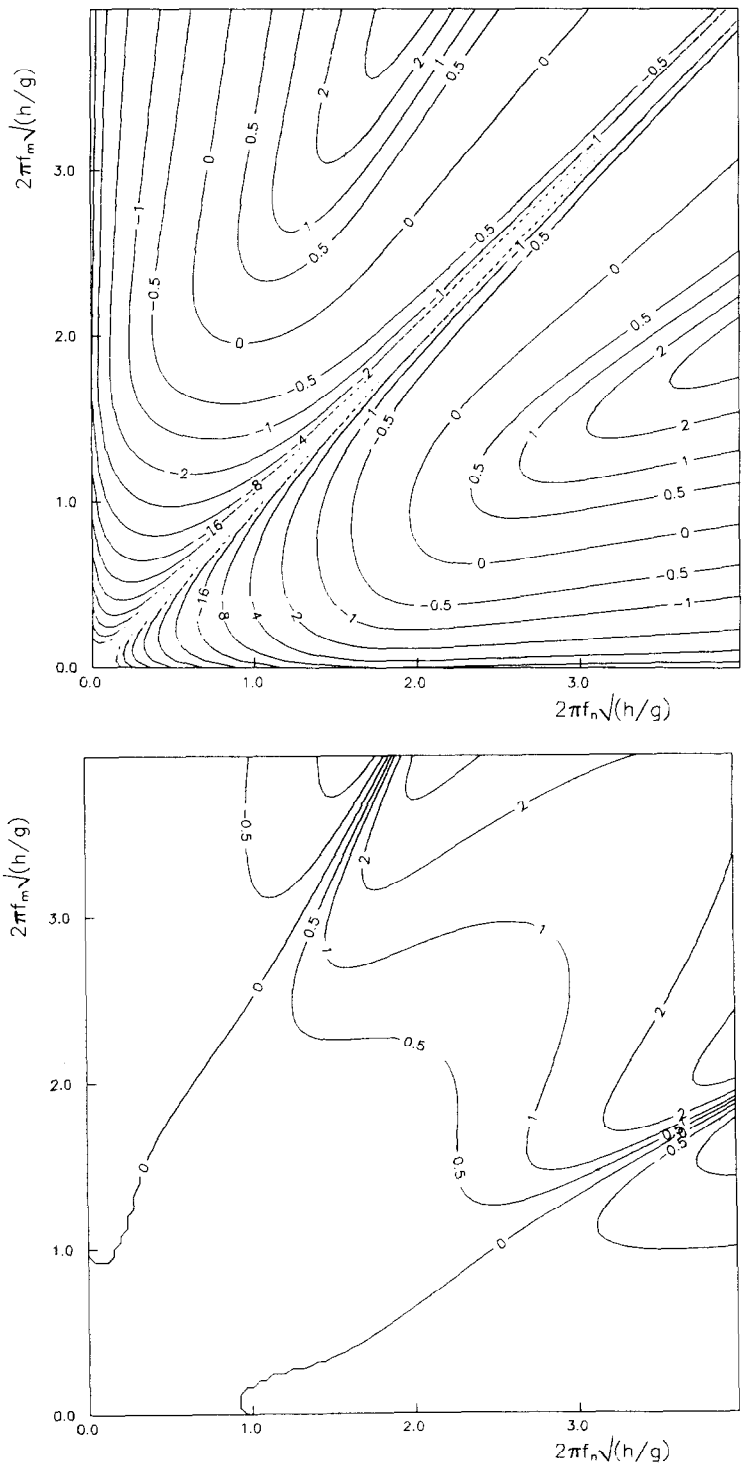


Fig. 6(a).

(b)

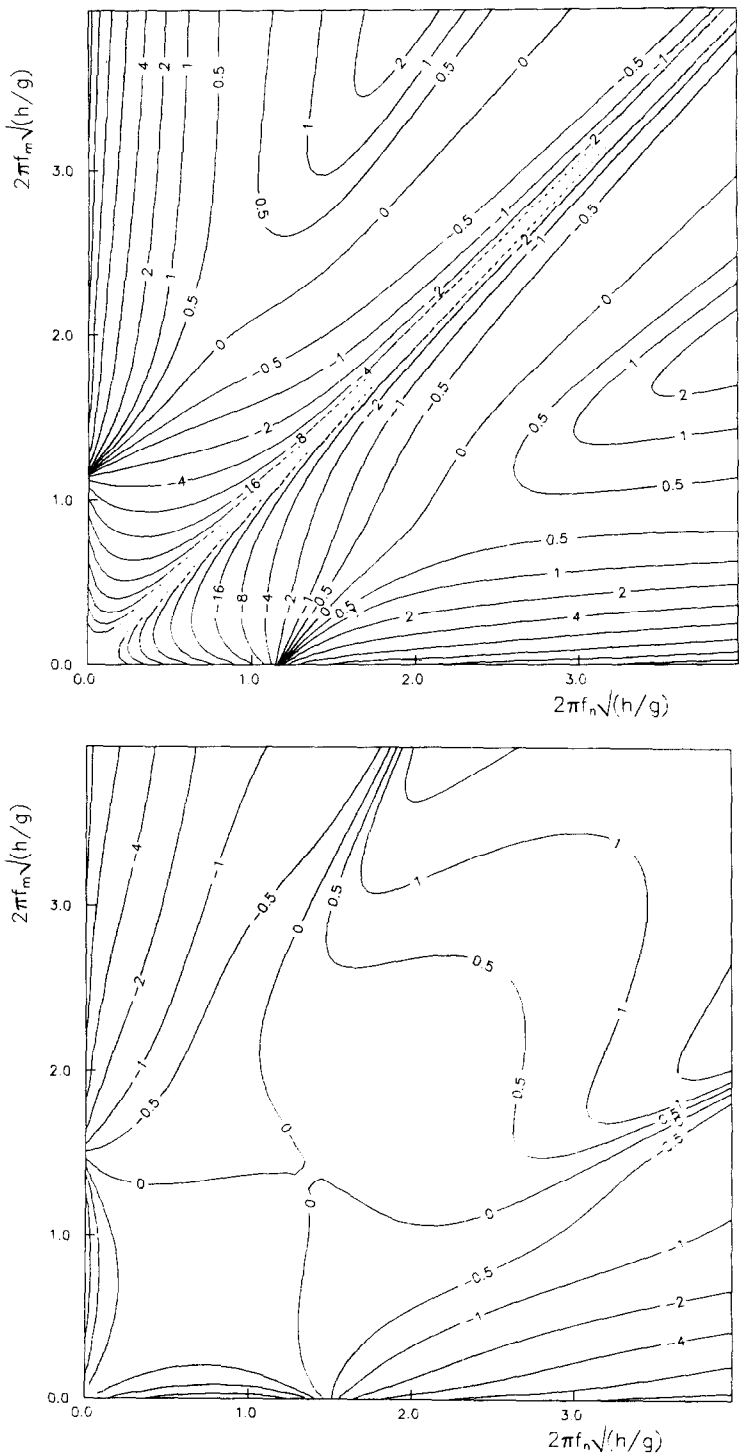


Fig. 6(b).

(c)

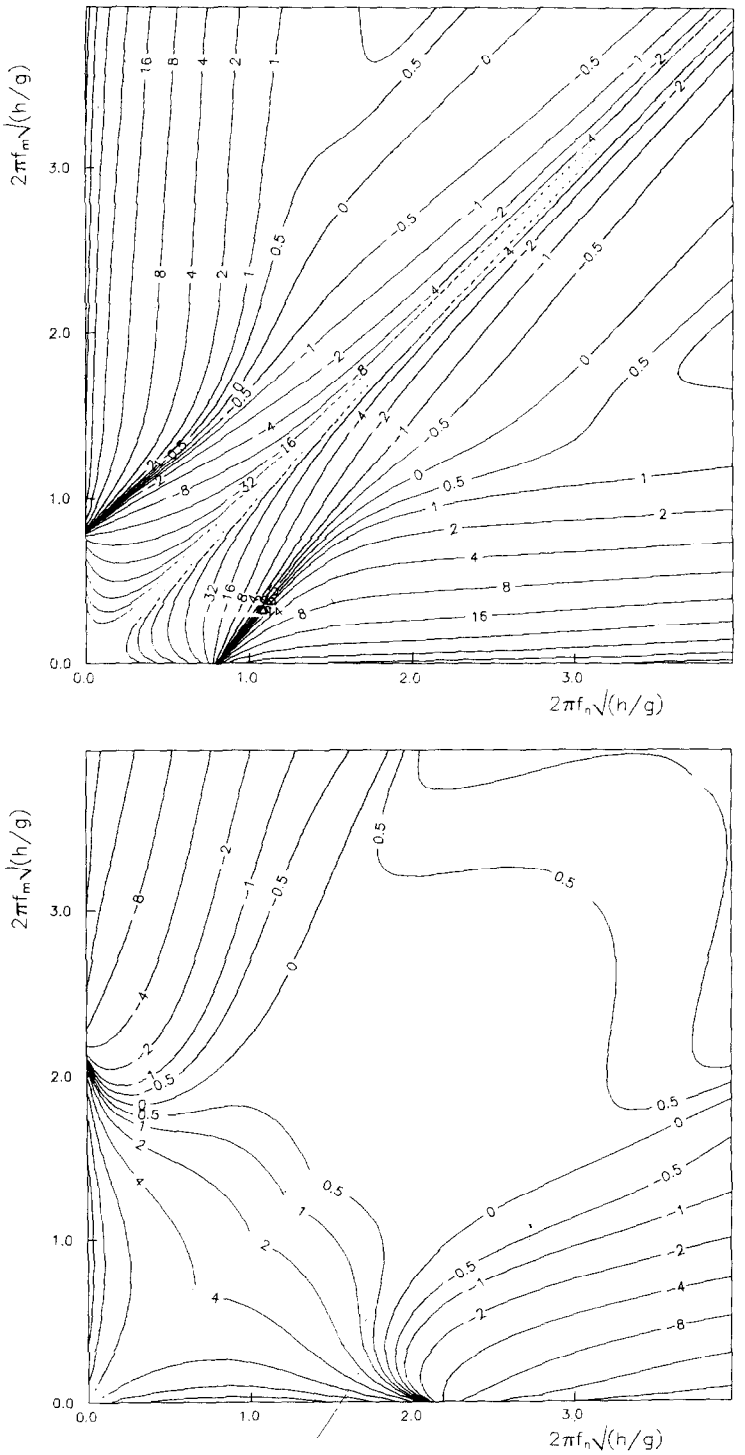


Fig. 6(c).

## 4. EXPERIMENTAL VERIFICATION

The experimental facility used is a 20 m flume, 1.0 m deep and 0.60 m wide, equipped with a piston-type wavemaker at one end ($x = 0$) and an efficient passive absorber at the other end. The absorber consisted of an array of vertical, perforated plates.

### 4.1. *Regular waves*

Six cases (see Table 1) were tested using generation correct to first and second order respectively.

For a depth of $h = 0.70$ m, a period of $T = 3.0$ s and a height of $H = 0.14$ m Figs 8 and 9 show time series of surface elevation at different positions in the flume using first-order and second-order control signals, respectively. The use of first-order wavemaker theory (Fig. 8) gives a spurious, free superharmonic, progressive wave generated wave component in addition to the natural, forced superharmonic. These two superharmonic wave components progress at different celerities creating an interference pattern resulting in different wave shapes throughout the flume, the repetition length (in this case) theoretically predicted to be 19.1 m. Close to the wavemaker ($x = 1.00$ m in Fig. 8) the two superharmonics almost cancel and the elevation becomes nearly sinusoidal, which is not a stable form for this rather nonlinear wave. Further down the flume this results in secondary peaks in the troughs. The use of second-order wavemaker theory solves these problems (see Fig. 9).

This test was used by Sand and Mansard to successfully verify their version of second-order wavemaker theory. The difference between the two theories is small for this rather shallow water example, but it is indeed significant in deeper water.

A detailed analysis was made using the following two steps for the surface elevation time series measured at each wave gauge (positions 1.00, 4.00, 4.40, and 8.70 m from the wavemaker): (1) band pass filtering around the primary frequency and the superharmonic frequency, respectively; and (2) zero-crossing of the filtered time series in order to obtain the respective wave heights.

For a wide range of periods, $T = 3.0$, 2.0, 1.5, 1.2, 1.0 and 0.8 s corresponding to water depth to wave length ratios, $h/L = 0.09$, 0.15, 0.22, 0.32, 0.45 and 0.7. As examples of the importance of the new terms in the transfer function we look at the periods $T = 3.0$, 2.0 and 1.2 s. The values of the complex transfer function $\mathcal{F}^+$ for these periods are (1.53, 0.00), (0.40, 0.03), and (0.18, 0.15). If the new terms corresponding to $F^+_{13}$, $F^+_{22}$ and $F^+_{22}$ are neglected these values become (1.46, −0.02), (0.25, −0.07) and (−0.17, −0.13). As expected, the new terms are important except near the shallow water limit. Even in the intermediate water depth (represented here by $T = 1.2$ s) the new terms change the original values by roughly −200%.

Figure 10 compares the experiments with theory. The solid curves are theoretical results and the experiments are given by white squares in case of first-order generation and black squares in case of second-order generation.

For the primary wave the constant wave height given by the solid line gives the

Fig. 6. (opposite) Components subharmonic complex transfer functions $\mathcal{F}^-/\delta_{nm}$ vs dimensionless first-order frequencies $2\pi f_n \sqrt{h/g}$ and $2\pi f_m \sqrt{h/g}$ for the same three wavemaker configurations as in Fig. 3. Contour lines are a subset of $(0, \pm 1/n, n = 1, 2, \ldots, 10 \ldots)$.

(a)

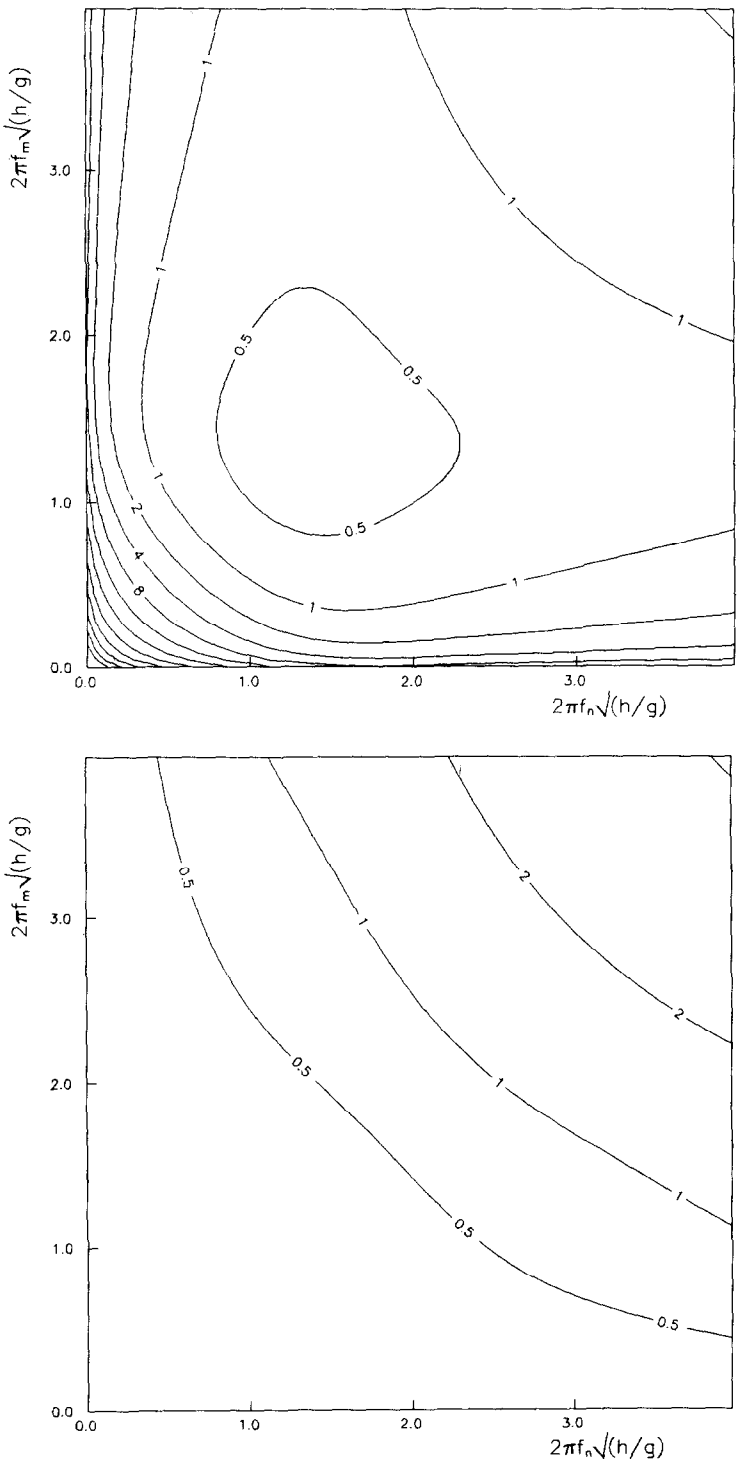


Fig. 7(a).

(b)

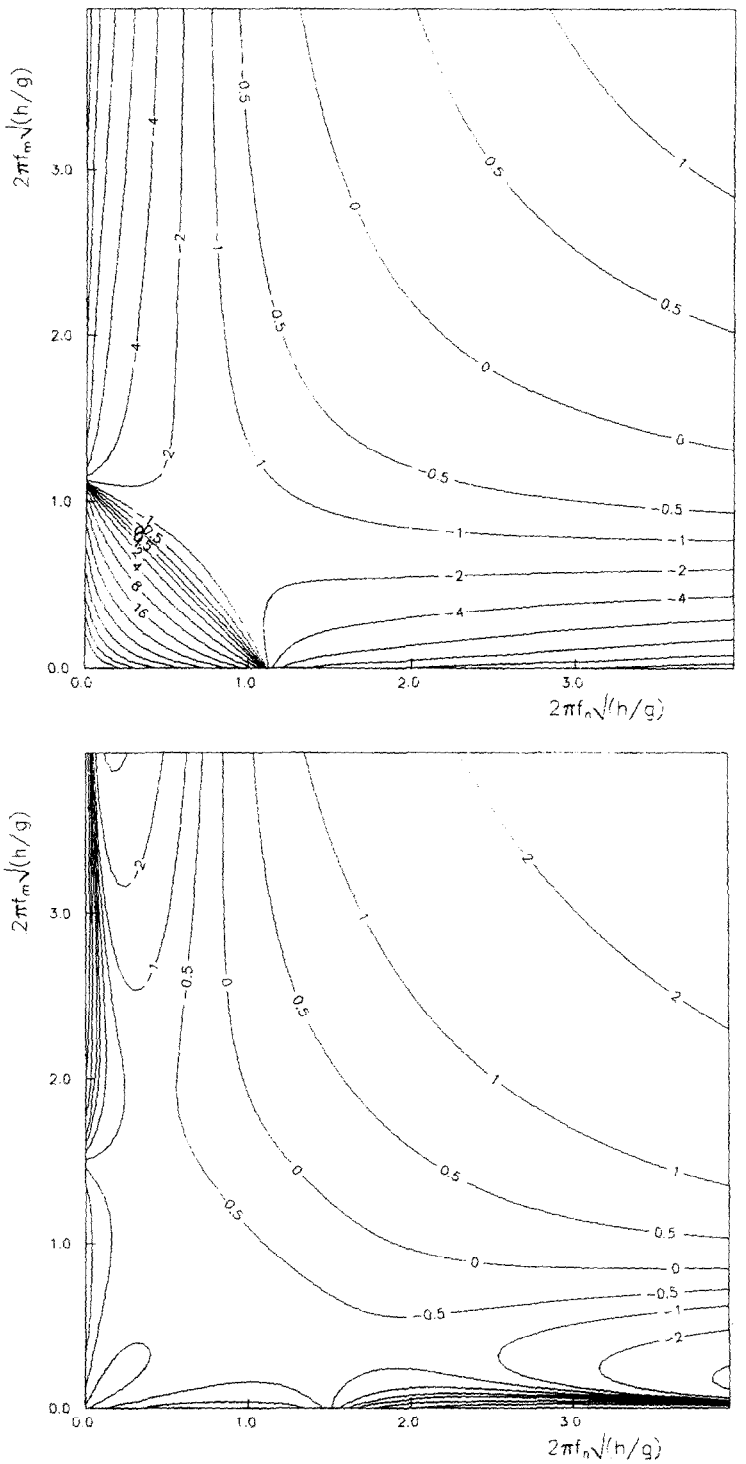


Fig. 7(b).

(c)

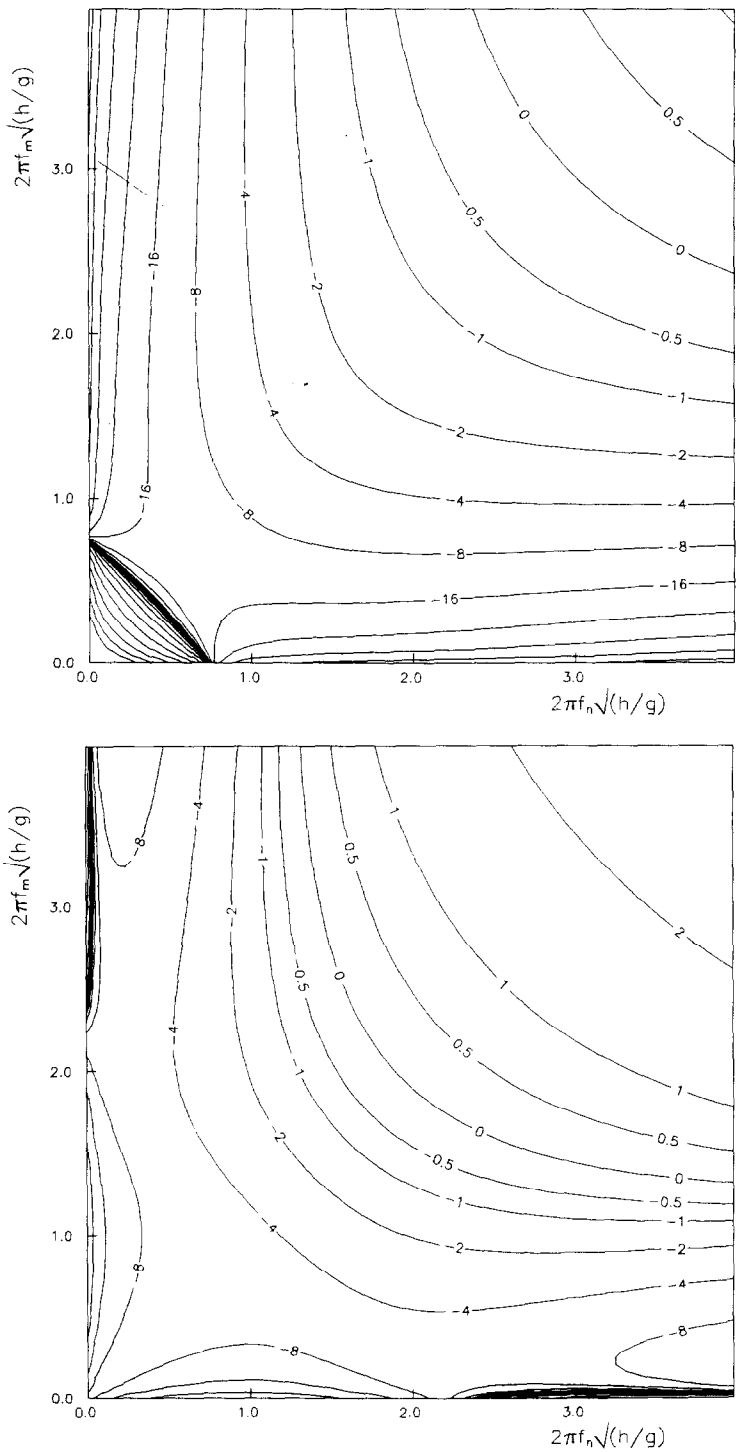


Fig. 7. As Fig. 6, but for $\mathcal{F}^+/\delta_{nm}$ corresponding to superharmonics.

Table 1. Regular wave experiments. $S$ (Equation 52) is based on $H$ and $G^{+}_{11}$

| Water depth $h$ (m) | Period $T$ (sec) | Wave height $H$ (m) | $kh$ | Nonlinearity parameter $S$ |
|---|---|---|---|---|
| 0.7 | 3.0 | 0.14 | 0.59 | 1.08 |
| 0.7 | 2.0 | 0.12 | 0.95 | 0.49 |
| 0.7 | 1.5 | 0.155 | 1.41 | 0.49 |
| 0.7 | 1.2 | 0.15 | 2.03 | 0.50 |
| 0.7 | 1.0 | 0.12 | 2.84 | 0.50 |
| 0.7 | 0.8 | 0.08 | 4.40 | 0.50 |

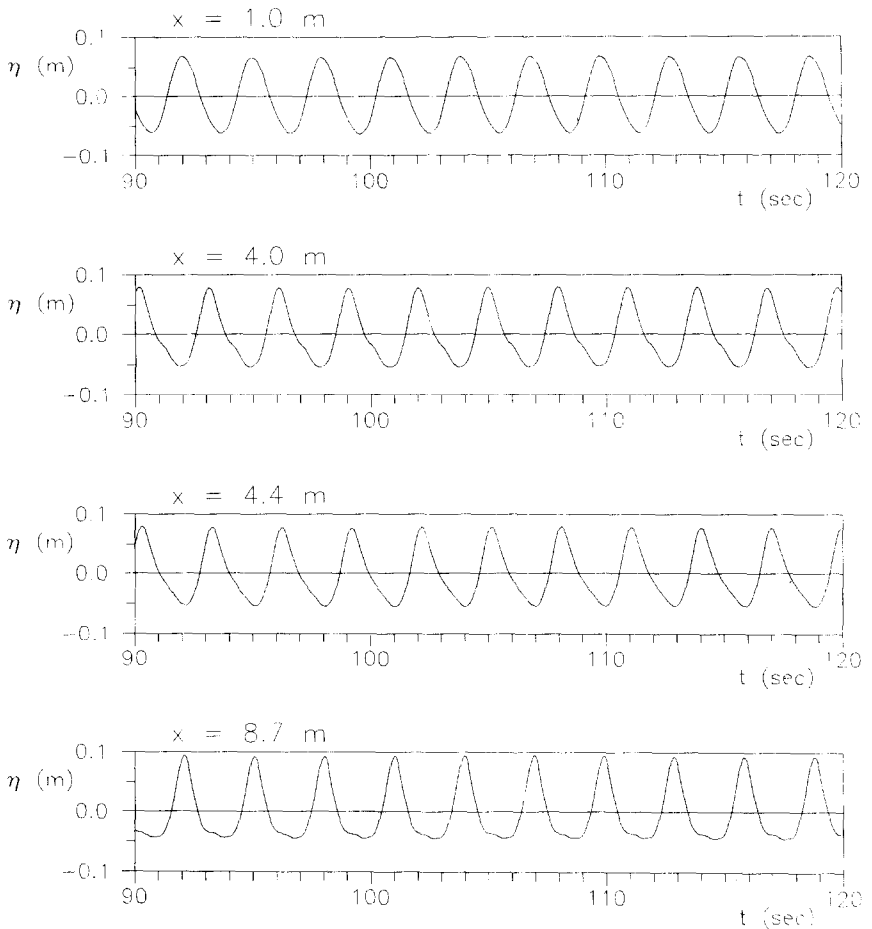


Fig. 8. Time series of surface elevation measured at different positions in the flume ($x = 0$ at the piston-type wavemaker) using a first-order control signal ($h = 0.70$ m, $T = 3.0$ s, and $H = 0.14$ m).

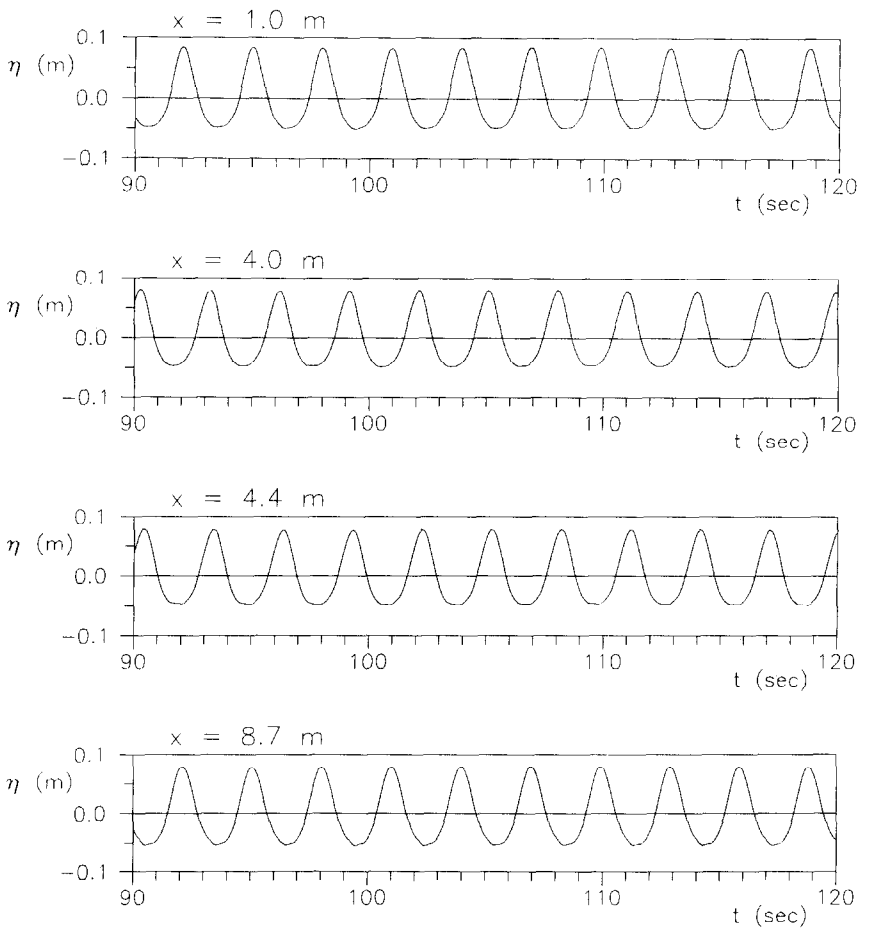


Fig. 9. As for Fig. 8, but using a second-order control signal.

specified wave height and the experimental values are seen to be somewhat smaller in most cases.

For the superharmonic the constant bound wave heights given by the straight lines are the theoretical values based on the specified primary wave height and the spatial mean of the measured primary wave heights, respectively. The black squares are expected to lie between these two lines and the agreement is satisfactory.

The oscillating curves give the second-order theoretical height of the interference wave pattern of bound and free superharmonic components resulting from first-order wave generation. Again, the upper curve is based on the specified primary wave height whereas the lower one is based on the spatial mean of the measured primary wave heights. The white squares are expected to lie between the two oscillating curves. The agreement is generally good.

The experiments clearly show how second-order wave generation gives waves of constant form as opposed to first-order generation (the black squares are far closer to being constant than the white squares). This conclusion holds even in deep water.

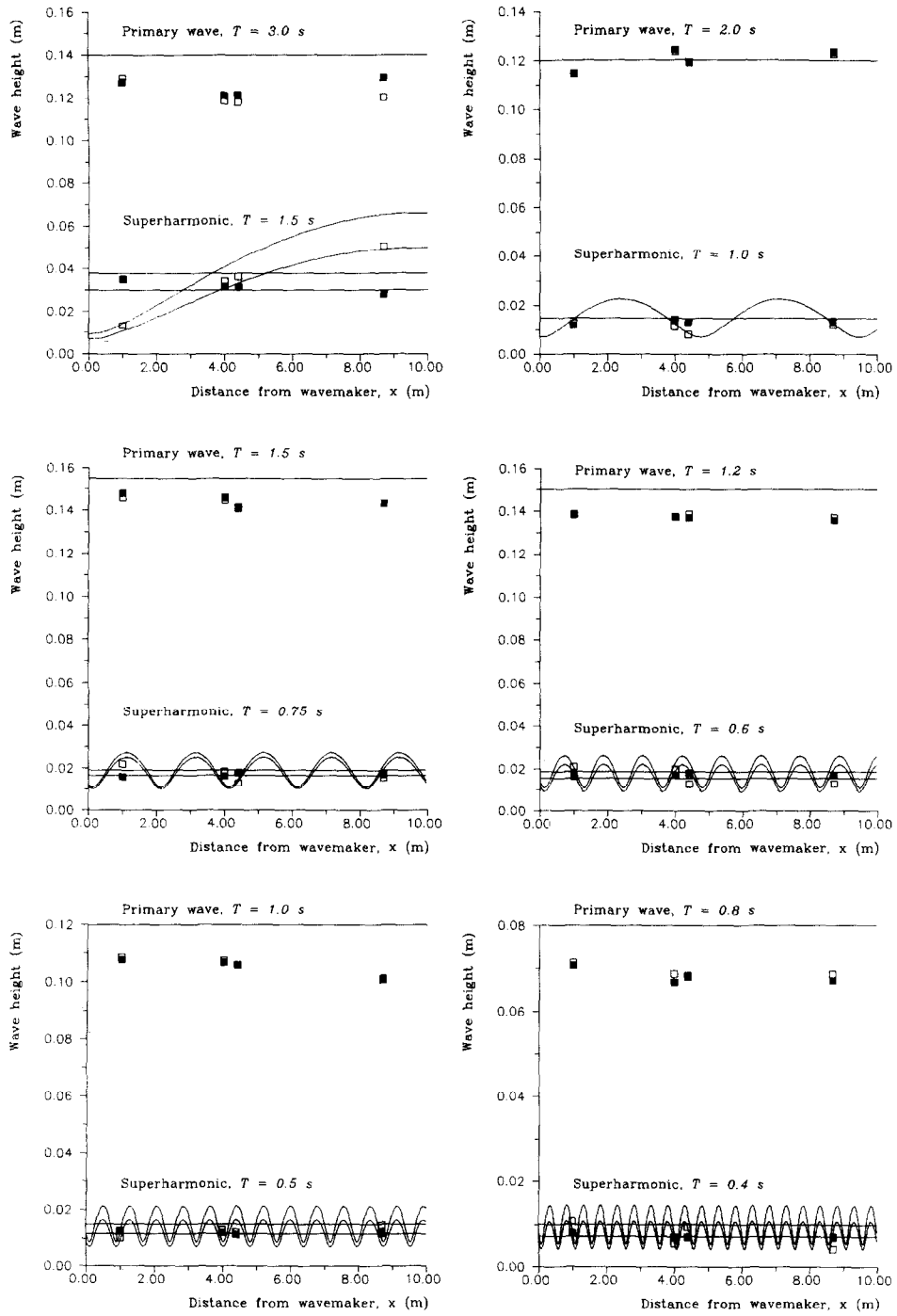


Fig. 10. Wave heights for the primary wave and the superharmonic using first-order control signal (white squares) and second-order control signal (black squares), respectively. Theory is indicated by the curves and the straight lines. For the superharmonic these give the second-order theory for generation correct to first- and second-order, respectively. The theory of the superharmonic is shown both for the specified and for the actually measured primary wave height (spatial mean). Water depth was $h = 0.70$ m and the wavemaker was of the piston type. See also Table 1.

### 4.2. *Wave groups*

Experiments for bichromatic primary waves were made in the same wave flume, but now with five wave gauges placed $x = 1.95$, 3.00, 6.00, 6.40 and 12.00 m from the wavemaker. Experiments were made with first-order generation and second-order generation, respectively, for five cases numbered according to Table 2. Cases 1 and 2 are adopted from Barthel *et al.* (1983) but reproduced in half the length scale of their experiments except for the flume length being only 20 m instead of half of their 67 m.

Although the second-order generation included both subharmonics and superharmonics we shall focus on the difference frequency and thus the parameter $S$ (52) in Table 2 was based on $G^{-}_{12}$ and $H = H_1 = H_2$.

A thorough investigation of the superharmonics was not pursued, since these were treated in detail under regular waves. However, since for bichromatic primary waves, we have terms at the frequency $f_1 + f_2$ which do not appear in regular waves, a brief indication of the validity of the theory is shown graphically. Using case 1 of Table 2, Fig. 11(a) and (b) shows a sequence of the elevation (low-pass filtered to remove the difference frequency components) measured at $x = 3.00$ m, with first- and second-order generation, respectively. Like for regular waves, the secondary peaks arising from spurious free superharmonics disappear when second-order generation is used.

When two frequencies are present in the primary wave train, long waves appear at second order and the experimental verification at these low subharmonic frequencies becomes somewhat more complicated. This is due to inevitable reflections (from the passive absorber) of bound or free, long waves at the difference frequency and their reflection at the wavemaker. [If a sloping beach had been used in place of the absorber the problem would have been that of surf beat generation, and reflection coefficients exceeding unity could have appeared; for example, see Schäffer (1993c).] As opposed to the superharmonic case, we can no longer assume all components to be progressive. In order to include all five measuring points, a least squares procedure was used for what is essentially a second-order reflection analysis. Assuming that, at the difference frequency, both bound and free waves are (partially) reflected from the absorber as free waves and subsequently fully re-reflected at the wavemaker, the long-wave field consists of a free, standing wave with antinode at the wavemaker in addition to the bound and free components produced by the wavemaker as for an infinitely long flume. This allows us to extract the essential components for the verification of the wave generation technique, i.e. the ones directly emitted from the wavemaker. These are

Table 2. Wave group experiments. $S$ (Equation 52) is based on $H = H_1 = H_2$ and $G^{-}_{12}$

| Case No. | Water depth $h$ (m) | Frequencies $F_1/F_2$ (Hz) | Wave heights $H_1/H_2$ (m) | $k_1h/k_2h$ | Nonlinearity parameter $S$ |
|---|---|---|---|---|---|
| 1 | 0.3 | 0.495/0.566 | 0.03/0.03 | 0.57/0.66 | 0.89 |
| 2 | 0.6 | 0.60/0.70 | 0.12/0.12 | 1.09/1.35 | 0.59 |
| 3 | 0.6 | 0.50/0.70 | 0.11/0.11 | 0.86/1.35 | 0.67 |
| 4 | 0.6 | 0.60/0.80 | 0.10/0.10 | 1.09/1.66 | 0.45 |
| 5 | 0.6 | 0.80/1.00 | 0.08/0.08 | 1.66/2.45 | 0.24 |

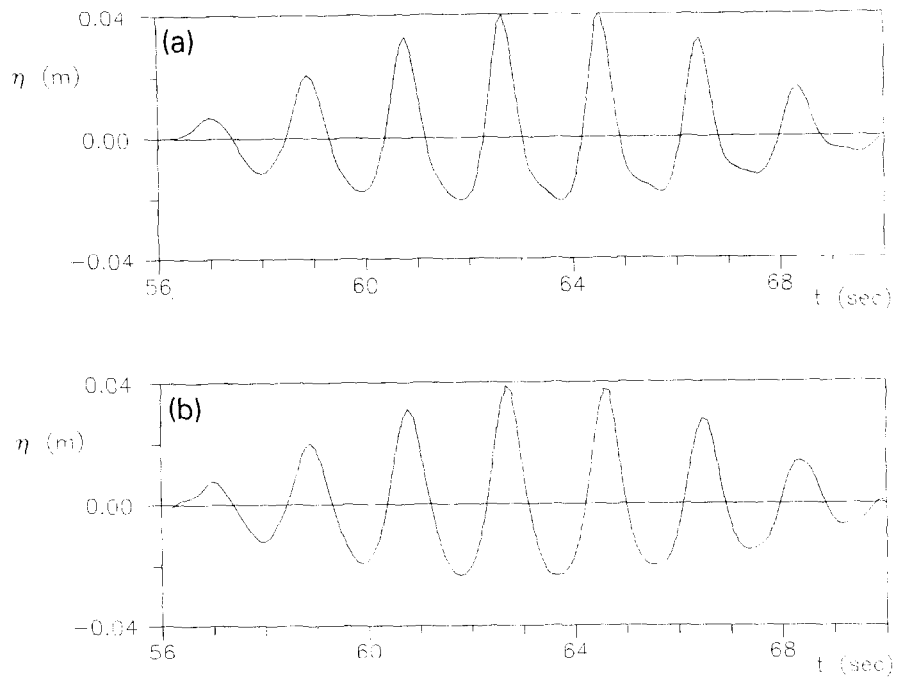


Fig. 11. Case 1 of Table 2. Visual demonstration of the capability of second-order wave generation to suppress spurious superharmonics also in case of bichromatic primary waves: (a) surface elevation with secondary peaks using first-order wave generation, and (b) "clean" peaked nonlinear waves with wide and flat troughs as generated with a second-order wavemaker control signal.

the bound, long waves, denoted $\eta_b$ and the spurious, free, long waves denoted $\eta_f$ in the following.

Before showing the results of the analysis providing the amplitude of $\eta_b$ and $\eta_f$ we shall present the data from cases 1 and 2 of Table 2 as done by Barthel *et al.* (1983). Close to $x = 6$ m ($x = 3$ m) the standing, free, long wave has a nodal point and thus it does not show up in the measured elevation. Thus, the low-frequency signal at this point is almost entirely constituted by $\eta_b$ and $\eta_f$, giving an indication of the performance of the applied wave generation technique. For case 1, Fig. 12(a) and (b) shows the difference frequency signal together with the surface elevation (low-pass filtered to remove the difference frequency components) using first- and second-order generation, respectively. While the long wave setdown, as it should, appears under the high primary waves when second-order generation is used [Fig. 12(b)], spurious, free, long waves spoil the picture in case of first-order generation [Fig. 12(a)]. These results are similar to those obtained by Barthel *et al.* (apart from the scaling factor of two) which is not surprising, since for this case the value of the transfer function compares well with their findings. In case 2, however, their theory predicted the difference frequency contribution to the second-order transfer function to vanish, and thus their results did not improve using second-order generation. This is in contrast to the present theory, for which the two cases are shown in Fig. 13(a) and (b). Although a phase relation

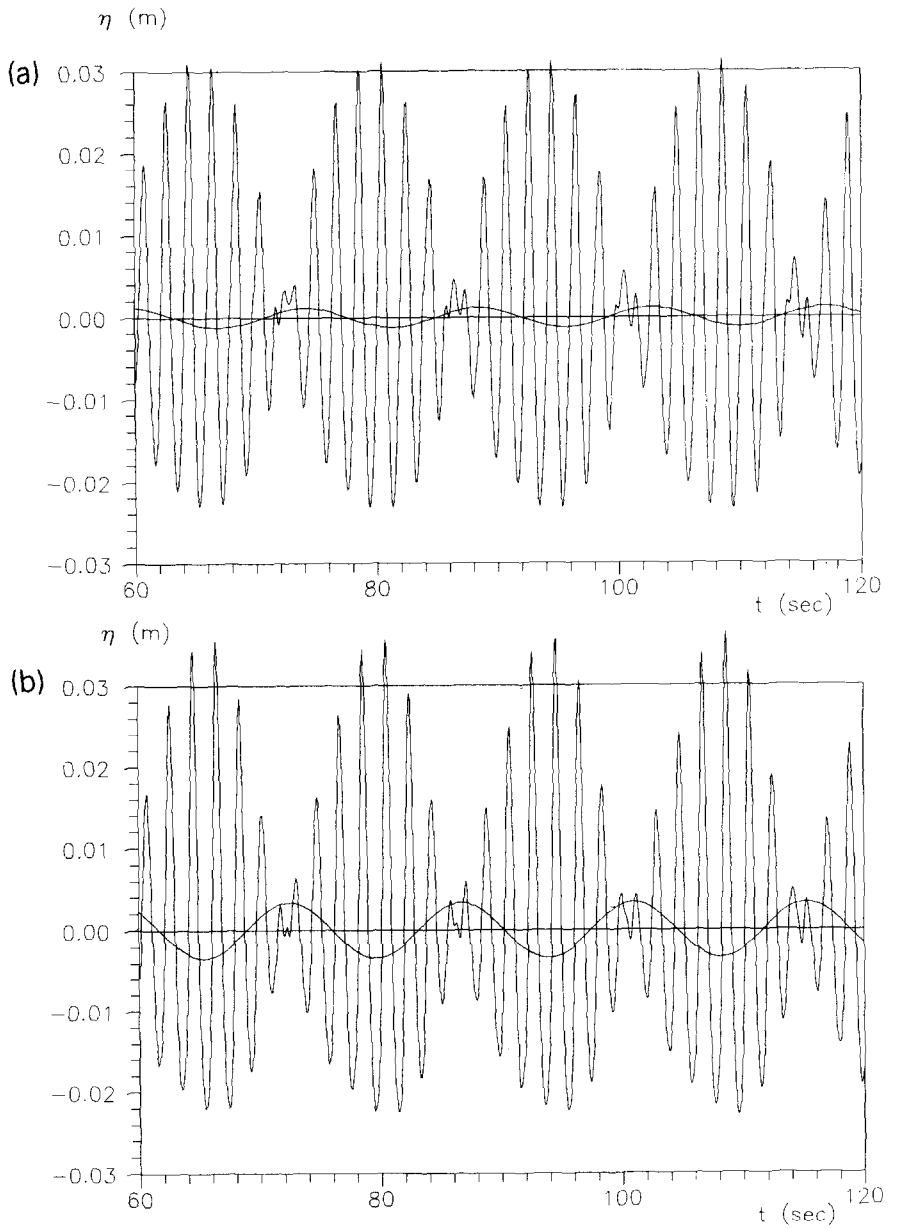


Fig. 12. Case 1 of Table 2. Visual demonstration of the capability of second-order wave generation to suppress spurious, free, long wave superharmonics in case of bichromatic primary waves. The difference frequency signal is shown together with the groups using (a) first-order generation, and (b) second-order generation.

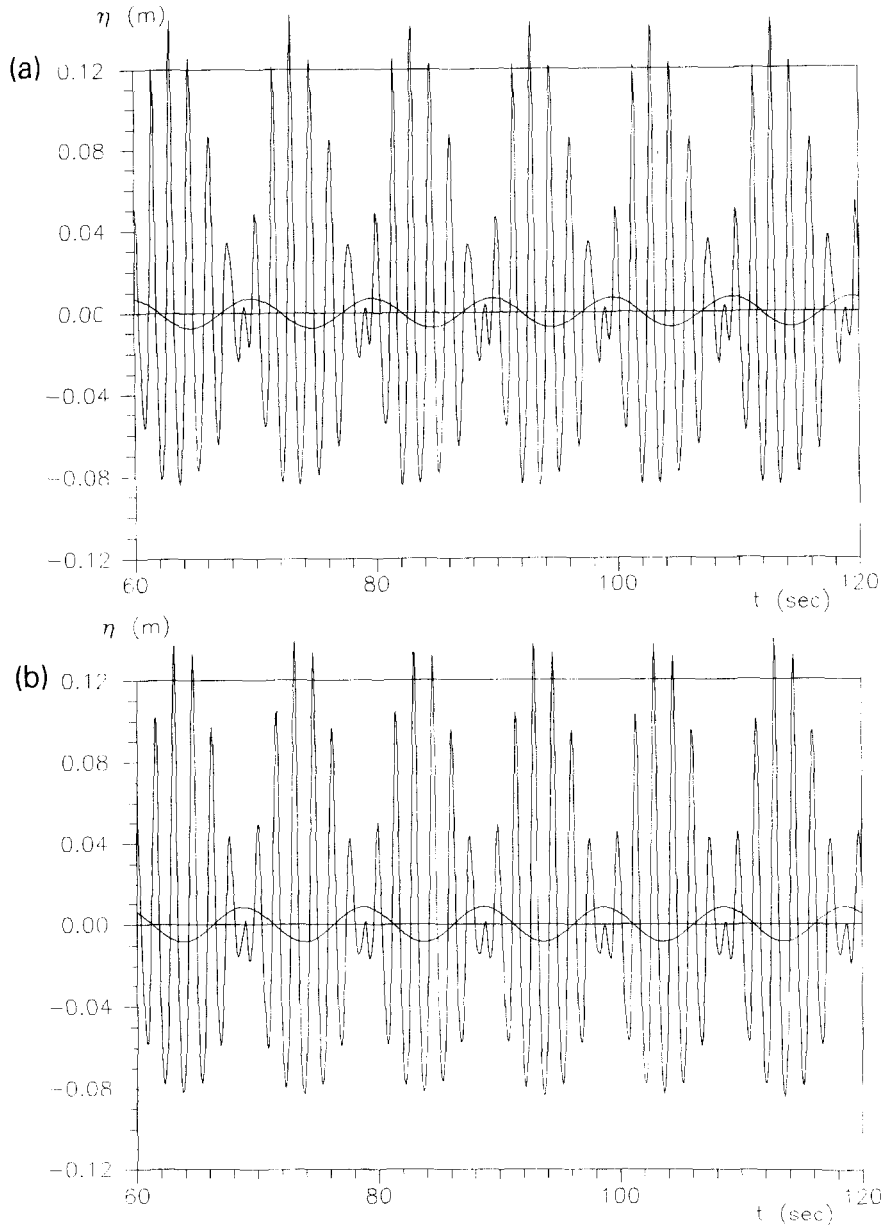


Fig. 13. As for Fig. 12, but for case 2 of Table 2.

between long waves and groups appears to be correct in Fig. 13(b) and slightly off in Fig. 13(a), this case is not quite as convincing as case 1 [Figs 12(a) and (b)]. However, this is due to the first-order generation appearing less bad rather than the second-order generation being less good. In fact the quantitative results from the second-order

reflection analysis shown below indicate that the use of second-order generation works better in case 2 than in case 1.

The bound, long waves $\eta_b$ appear irrespective of the order of the control signal used for the wavemaker. Figure 14(a) compares the experimental and theoretical values of the amplitude of $\eta_b$. As before, black squares indicate second-order wave generation and here they almost cover the white squares, which indicate first-order generation. It appears that $\eta_b$ is generally a little overpredicted by the theory. The labels refer to the numbering of cases of Table 2, and it appears that generally the larger the nonlinearity parameter $S$ the larger is the overprediction.

Using second-order wave generation the amplitude of $\eta_f$ as indicated by the black squares in Fig. 14(b) should ideally vanish, and they are in fact quite small. Again the less good results appear when nonlinearity is large and it is pleasing to see that the amplitudes of $\eta_f$ are generally comparable to the difference between theoretical and experimental amplitudes of $\eta_b$. The second-order wavemaker theory can also be used for predicting the amplitude of $\eta_f$ when first-order generation is applied. The comparison with the experimental values is indicated by the white squares in Fig. 14(b). Despite the scatter, the results clearly support the present theory.

### 4.3. *Irregular waves*

Using the same experimental set-up as for the wave groups, but now with five wave gauges placed $x$ = 1.40, 5.75, 8.45, 12.25 and 13.50 m from the wavemaker, two cases (see Table 3) of irregular waves were generated using first- and second-order generation, respectively. The primary waves were synthesized using the inverse FFT approach with random phase assignment for JONSWAP spectra with a peak enhancement factor $\gamma$ = 3.3. The second-order correction to the wavemaker control signal was computed

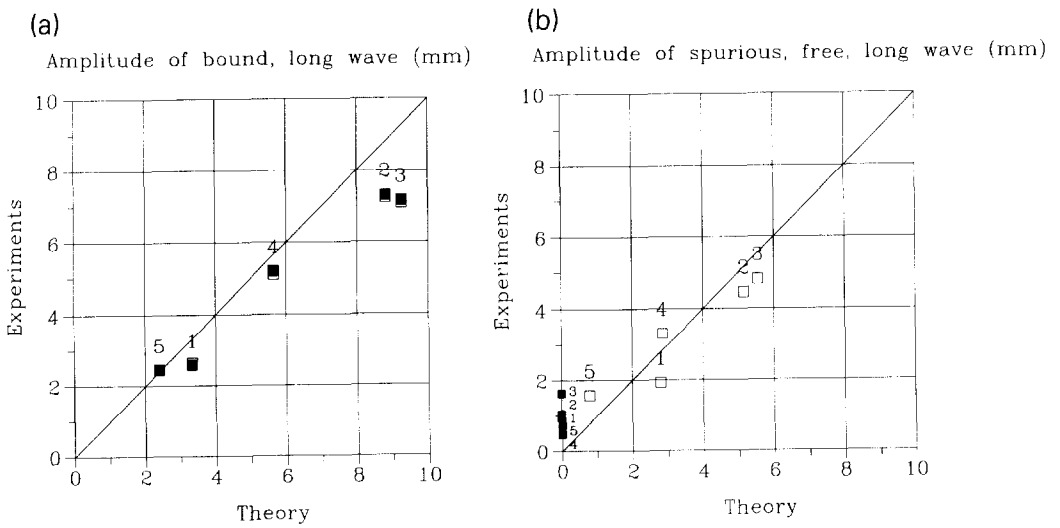


Fig. 14. All five cases of Table 2, with white squares for first-order generation and black squares for second-order generation. Comparison between theory and experiments for amplitudes of (a) bound, long waves, and (b) free, long waves.

Table 3. Irregular wave experiments. $S$ (Equation 52) is based on $H_s$ and $G^+_{nm}$ at $(f_p, f_p)$

| Water depth $h$ (m) | Peak frequency $f_p$ (Hz) | Significant wave height $H_s$ (m) | $k_p h$ | Nonlinearity parameter $S$ |
|---|---|---|---|---|
| 0.3 | 0.59 | 0.05 | 0.70 | 0.69 |
| 0.3 | 0.73 | 0.06 | 0.90 | 0.61 |

deterministically from each pair of interacting primary wave components starting in the frequency domain and applying the inverse FFT. The record length was 10 min and the computing time for the first- and second-order control signals was 28 sec on a fast PC (66 MHz 486). The peak frequencies, the depth, and the wave gauge locations were the same as for the two irregular-wave experiments carried out by Barthel *et al.* (1983), except for being in half the length scale of their experiments.

The method of analysis used in connection with wave groups is not applicable for irregular waves, since many pairs of interacting first-order components contribute to the activity at each difference frequency. Thus, even if we were to analyse each difference frequency separately, there would be a whole spectrum of wave lengths for the bound, long waves, and thus no simple harmonic spatial variation.

Thus, we chose to live with the distortions of the progressive wave signals appearing from reflections from the absorber and their re-reflections from the wave paddle.

The measured elevations were low-pass filtered cutting at half the peak period. This signal is denoted $\eta_l$ in the following. For comparison the theoretical bound, long wave elevations, $\eta_b$, were obtained by similarly filtering the bound subharmonic signals. For the first case in Table 3, Fig. 15 compares $\eta_l$ (solid curve) with $\eta_b$ using wave

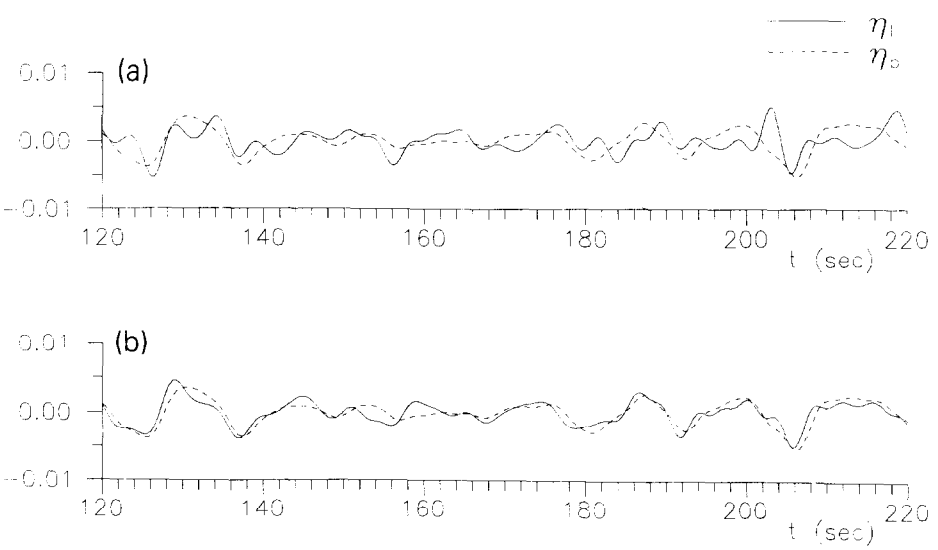


Fig. 15. Sample comparison of low-pass filtered surface elevation $\eta_l$ and theoretical bound, long waves $\eta_b$ for the first case of Table 3, using (a) first-order generation, and (b) second-order generation. The solid curves give the experimental data.

generation correct to first-order and second-order, respectively. The example is taken at $x = 12.25$ m, between $t = 120$ and 220 s out of a 10-min record. Clearly second-order generation gives the best fit. Remember though, that spurious long-wave reflections distort the measured signals and a very close fit to theory is not to be expected. Even when first-order wave generation is applied, similarities between $\eta_l$ and $\eta_b$ can be found. This is consistent with the fact that bound, long waves are generated regardless of the order of the wave generation, the difference between first- and second-order being that additional spurious, free, long waves are emitted from the wavemaker in case of first-order wave generation. The results given in Fig. 15 are similar to the ones obtained by Barthel *et al.* (1983). In the second case of Table 3, however, Barthel *et al.* did not obtain better results using their second-order wave generation. Figure 16 shows the comparison in this second case and it appears that now second-order generation gives a similar improvement as seen in the first case. This supports the idea that the problems of the previous theory have been resolved in the present formulation.

Finally we want to get a quantitative measure of the above comparison including all five gauges and the full 10 min record of the experiments. This is done by computing the sample cross-correlation coefficient function $\rho_{xy}$ taking $\eta_l$ as $x$ and $\eta_b$ as $y$. For the two cases in Table 3 the results are shown in Figs 17 and 18, respectively. It appears that for both cases the maximum of $\rho_{xy}$ is around 0.75 using second-order generation and only 0.5 or less using the first-order generation. Due to spurious free-wave reflections at the absorber and subsequent re-reflections at the wave paddle, it is to be expected that even for second-order generation the maximum values of $\rho_{xy}$ do not get very close to unity. Since bound waves are generated even in case of first-order generation $\rho_{xy}$ is expected to have a maximum close to zero lag even in this case. However, this maximum should be significantly smaller than for second-order wave generation and Figs 15 and 16 show that this is indeed the case. Note that for first-order generation,

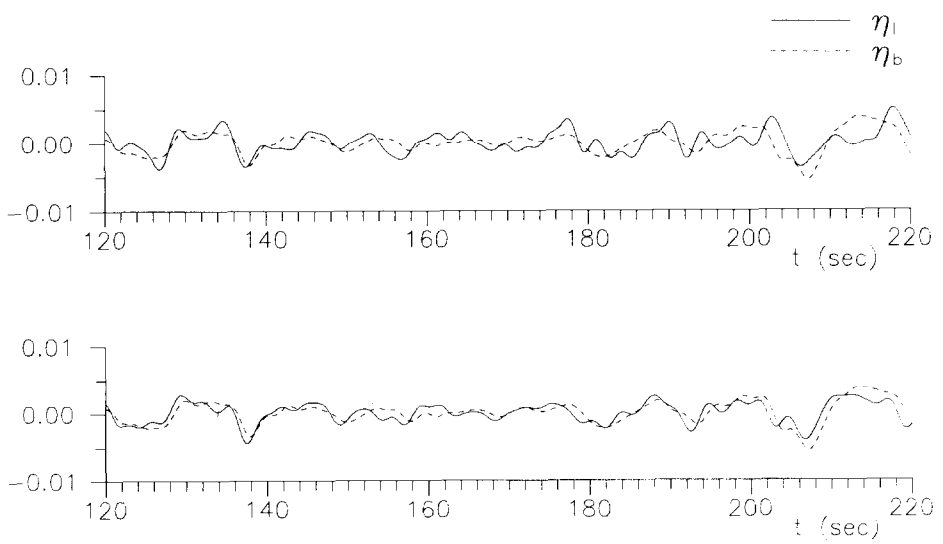


Fig. 16. As for Fig. 15, but for the second case of Table 3.

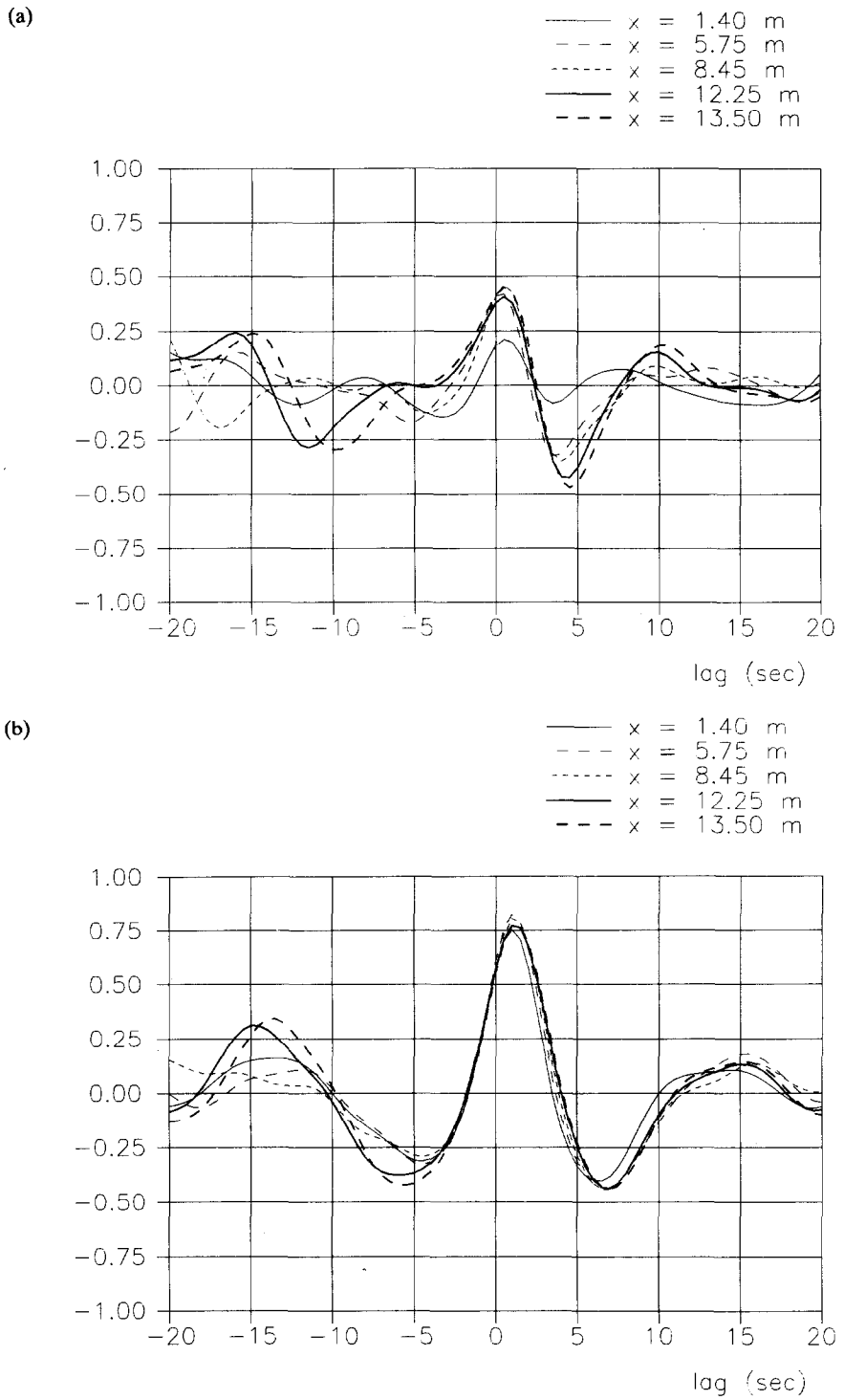


Fig. 17. Cross-correlation coefficient function $\rho_{xy}$ taking the low-pass filtered surface elevation $\eta_l$ as $x$ and the (similarly filtered) theoretical bound long wave elevation, $\eta_b$ as $y$ for the first case of Table 3, using (a) first-order generation, and (b) second-order generation.

(a)

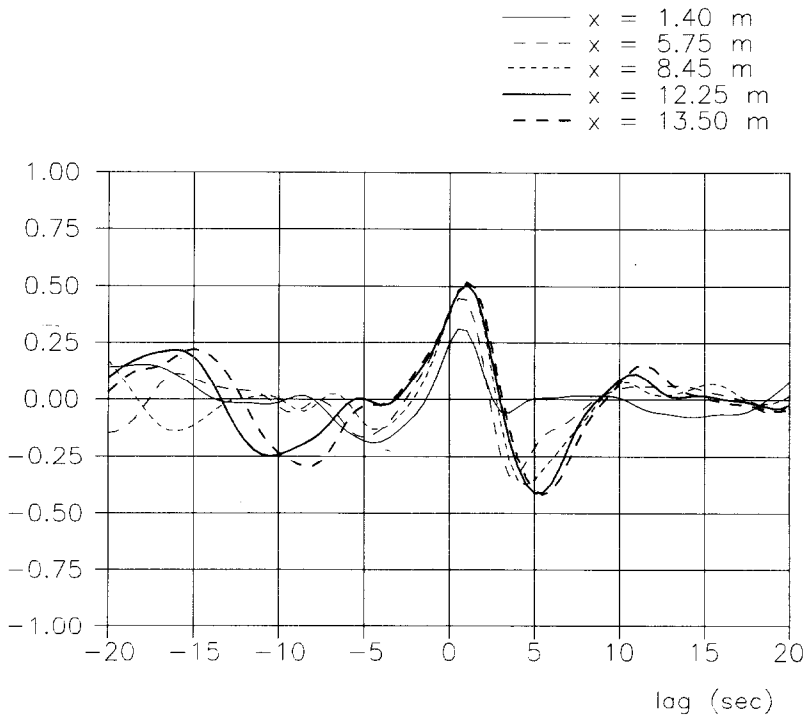


(b)

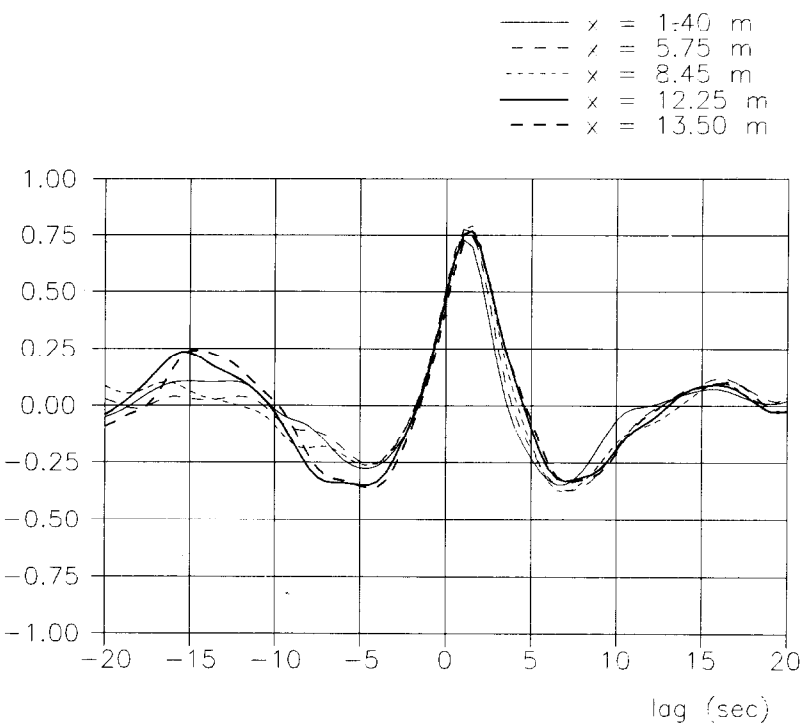


Fig. 18. As for Fig. 17, but for the second case of Table 3.

the maximum of $\rho_{xy}$ is comparatively small at the position close to the wavemaker ($x = 1.40$ m). Since the bound, long waves and the spurious, free, long waves tend to cancel each other close to the wavemaker in case of first-order wave generation, this is in qualitative agreement with the theory.

Finally, we note, that in all cases Figs 15 and 16 show that the theory lags the measurements by slightly over 1 sec. This may in part be attributed to amplitude dispersion of the primary waves, which is of course not included in the second-order theory. This phenomenon shows up as the difference in lag at the different positions and it can be seen for the decreasing $\rho_{xy}$ in the range between 1 and 4 sec lags, showing increasing lags at increasing distances from the wavemaker.

## 5. SUMMARY AND CONCLUSIONS

A full second-order theory for the generation of waves by a rotating, translatory or combined wave board motion has been developed. Apart from being restricted by the inevitable limitations of usual second-order Stokes wave theory, this wavemaker theory involves no simplified assumptions, such as shallow water, small evanescent-mode interactions, or narrow-banded wave spectra. The primary result of the theory is given in terms of second-order transfer functions relating the first-order waves to the second-order wavemaker control signal. Using a control signal correct to second-order, spurious, free, superharmonics and subharmonics can be avoided.

Another application of the theory is to predict spurious free-wave generation when first-order control signals are used.

Using a piston-type wavemaker, a number of laboratory wave experiments for regular waves, wave groups, and irregular waves were conducted. In all experiments the results support the theory.

*Acknowledgements*—Jesper Skourup checked the theoretical development, Peter Hyllested included the second-order routines in the DHI Wave Synthesizer, and Niels Mathiesen assisted with the experiments. Financial support was granted from the Danish Energy Agency under the EFP'93 programme and from the Danish Technical Research Council (STVF) under the programme "Marin Teknik".

## REFERENCES

Barthel, V., Mansard, E.P.D., Sand, S.E. and Vis, F.C. 1983. Group bounded long waves in physical models. *Ocean Engng* **10,** 261–294.

Biésel, F. 1951. Etude théorique d'un type d'appareil à houle. *La Houille Blanche* **6,** 152–165.

Bowers, E.C. 1988. Wave grouping and harbour design. *Proc. Instn Civ. Engrs,* Part 2, **85,** 237–258.

Buhr Hansen, J., Schiolten, P. and Svendsen, I.A. 1975. Laboratory generation of waves of constant form. *Series Paper* **9,** Inst. of Hydrodyn. and Hydraulic Engng (ISVA), Tech. Univ. of Denmark, 56 pp.

Dean, R.G. and Sharma, J.N. 1981. Simulation of wave systems due to non-linear directional spectra. *Proc. Int. Symp. Hydrodynamics in Ocean Engng, The Norwegian Inst. of Technol.* **2,** 1211–1222.

Flick, R.E. and Guza, R.T. 1980. Paddle generated waves in laboratory channels. *J. WatWays, Port, Coastal Ocean Div., ASCE* **106**(WW1), 79–97.

Fontanet P. 1961. Théorie de la génération de la houle cylindrique par un batteur plan. *La Huille Blanche* **16,** 3–31 (part 1) and 174–196 (part 2).

Havelock, T.H. 1929. Forced surface waves on water. *Phil. Mag.*, Series 7, 569–576.

Hudspeth, R.T. and Sulisz, W. 1991. Stokes drift in two-dimensional wave flumes. *J. Fluid Mech.* **230,** 209–229.

Klopman, G. and Van Leeuwen, P.J. 1990. An efficient method for the reproduction of non-linear random waves. *Proc. 22nd Int. Conf. Coastal Engng.,* Delft, The Netherlands, 1990, ASCE, New York, 1991, **1,** 478–488.

Longuet-Higgins, M.S. and Stewart, R.W. 1962. Radiation stress and mass transport in gravity waves with application to "surf beats". *J. Fluid Mech.* **13,** 481–504.

Longuet-Higgins, M.S. and Stewart, R.W. 1964. Radiation stresses in waterwaves: a physical discussion with applications. *Deep Sea Res.* **11**, 529–562.
Madsen, O.S. 1971. On the generation of long waves. *J. Geophys. Res.* **76,** 8672–8673.
Mansard, E.P., Barthel, V., Funke, E.R., Klinting, P. and Jensen, O.J. 1989. Wave grouping and harbour design—discussion of Bowers (1988). *Proc. Instn Civ. Engrs,* Part 2, **87,** 135–142.
Mansard, E.P.D., Sand, S.E. and Klinting, P. 1987. Sub- and superharmonics in natural waves. *Proc. Offshore Mechanics and Arctic Engng*, Houston, Texas, pp. 83–89.
Moubayed, W.I. and Williams, A.N. 1994. Second-order bichromatic waves produced by a generic planar wavemaker in a two-dimensional wave flume. *J. Fluids Struct.* **8,** 73–92.
Ottesen Hansen, N.-E. 1978. Long period waves in natural wave trains. *Prog. Rep.* **46,** Inst. of Hydrodyn. and Hydraulic Engng. (ISVA), Tech. Univ. of Denmark, pp. 13–24.
Sand. S.E. 1982. Long wave problems in laboratory models. *J. WatWays, Port, Coastal Ocean Div., ASCE* **108**(WW4), 492–503.
Sand, S.E. and Donslund, B. 1985. Influence of wave board type on bounded long waves. *J. Hydraulic Res.* **23,** 147–163.
Sand, S.E. and Mansard, E.P.D. 1986a. Description and reproduction of higher harmonic waves. National Research Council of Canada, Hydraulics Laboratory Tech. Rep. TR-HY-012.
Sand, S.E. and Mansard, E.P.D. 1986b. Reproduction of higher harmonics in irregular waves. *Ocean Engng* **13,** 57–83.
Schäffer, H.A. 1993a. Laboratory wave generation correct to second order. *Proc. Int. Conf. Wave Kinematics and Environmental Forces,* London, 1993, Society for Underwater Technology, **29**.
Schäffer, H.A. 1993b. Second order irregular-wave generation in flumes—Computation of transfer functions by an asymptotic summation method. *Proc. Waves '93: 2nd Int. Symp. Ocean Wave Measurement and Analysis,* New Orleans, LA, U.S.A.
Schäffer, H.A. 1993c. Infragravity waves induced by short-wave groups. *J. Fluid Mech.* **247,** 551–588.
Schäffer, H.A. 1994. The influence of evanescent modes in second order wave generation. *Proc. Waves—Physical and Numerical Modelling,* Vancouver, B.C., Canada.
Sharma, J.N. 1979. Development and evaluation of a procedure for simulating a random directional second-order sea surface and associated wave forces. Ph.D. Dissertation, University of Delaware, 139 pp.
Suh, K. and Dalrymple, R.A. 1987. Directional wavemaker theory: a spectral approach. *Proc. IAHR-Seminar Wave Analysis and Generation in Laboratory Basins,* Lausanne, Switzerland, pp. 389–395.
Sulisz, W. and Hudspeth, R.T. 1993. Complete second-order solution for water waves generated in wave flumes. *J. Fluid Struct.* **7,** 253–268.
Svendsen, I.A. 1985. Physical modelling of water waves. In *Physical Modelling in Ocean Engineering* (Edited by R.A. Dalrymple). A. A. Balkema, Rotterdam.
Stokes, G.G. 1847. On the theory of oscillatory waves. *Trans. Camb. Phil. Soc.* **8,** 441–455.
Ursell, R., Dean, R.G. and Yu, Y.S. 1960. Forced small amplitude water waves: a comparison of theory and experiment. *J. Fluid Mech.* **7,** 32–52.

## APPENDIX

The functions $\Gamma_{1\ldots4}$ [see Equation (35)] are evaluated in this Appendix.

In order to reduce the computational cost for the case of irregular waves it is important to avoid terms like $\sinh(k_{0n} \pm k_{0m})h$, since these would have to be computed $\propto N^2$ times, where $N$ is the number of frequencies representing the first-order spectrum, whereas terms like $\sinh k_{0n}h$ need only be computed $\propto N$ times, provided that the sufficient computer memory is available.

For $\kappa_1 \neq \kappa_2$ we get

$$\Gamma_1(\kappa_1,\kappa_2) \equiv \int_{-h}^{0} \cosh \kappa_1(z+h) \cosh \kappa_2(z+h)\, dz$$
$$= \gamma_1(\kappa_1,\kappa_2;h), \tag{A1}$$

where

$$\gamma_1(\kappa_1,\kappa_2;r) \equiv \frac{\sinh(\kappa_1-\kappa_2)r}{2(\kappa_1-\kappa_2)} + \frac{\sinh(\kappa_1+\kappa_2)r}{2(\kappa_1+\kappa_2)}$$
$$= \frac{\cosh \kappa_1 r \cosh \kappa_2 r}{\kappa_1^2-\kappa_2^2}\left\{\kappa_1 \tanh \kappa_1 r - \kappa_2 \tanh \kappa_2 r\right\}. \tag{A2}$$

Furthermore,

$$\Gamma_2(\kappa_1,\kappa_2) \equiv \int_{-h+d}^{0} f(z)\cosh\kappa_1(z+h)\cosh\kappa_2(z+h)\,\mathrm{d}z$$
$$= \gamma_1(\kappa_1,\kappa_2;h) - \frac{1}{h+l}\left\{\gamma_2(\kappa_1,\kappa_2;h) - \gamma_2(\kappa_1,\kappa_2;d)\right\}, \tag{A3}$$

where

$$\gamma_2(\kappa_1,\kappa_2;r) = \frac{\cosh(\kappa_1-\kappa_2)r}{2(\kappa_1-\kappa_2)^2} + \frac{\cosh(\kappa_1+\kappa_2)r}{2(\kappa_1+\kappa_2)^2}$$
$$= \frac{\cosh\kappa_1 r\cosh\kappa_2 r}{(\kappa_1^2-\kappa_2^2)^2}\left\{\kappa_1^2+\kappa_2^2-2\kappa_1\kappa_2\tanh\kappa_1 r\tanh\kappa_2 r\right\} \tag{A4}$$

and

$$\Gamma_3(\kappa_1,\kappa_2) \equiv \int_{-h+d}^{0} \sinh\kappa_1(z+h)\cosh\kappa_2(z+h)\,\mathrm{d}z$$
$$= \gamma_3(\kappa_1,\kappa_2;h) - \gamma_3(\kappa_1,\kappa_2;d), \tag{A5}$$

where

$$\gamma_3(\kappa_1,\kappa_2;r) \equiv \frac{\cosh(\kappa_1-\kappa_2)r}{2(\kappa_1-\kappa_2)} + \frac{\cosh(\kappa_1+\kappa_2)r}{2(\kappa_1+\kappa_2)}$$
$$= \frac{\cosh\kappa_1 r\cosh\kappa_2 r}{\kappa_1^2-\kappa_2^2}\left\{\kappa_1 - \kappa_2\tanh\kappa_1 r\tanh\kappa_2 r\right\} \tag{A6}$$

by which

$$\Gamma_4(\kappa_1,\kappa_2) \equiv \kappa_1\Gamma_2(\kappa_1,\kappa_2) + \frac{1}{h+l}\Gamma_3(\kappa_1,\kappa_2)$$
$$= \frac{\cosh\kappa_1 h\cosh\kappa_2 h}{\kappa_1^2-\kappa_2^2}\left\{\kappa_1\tanh\kappa_1 h - \kappa_2\tanh\kappa_2 h\right.$$
$$- \frac{1}{h+l}\frac{\kappa_2/\kappa_1}{\kappa_1^2-\kappa_2^2}\left(2\kappa_1\kappa_2\left(1-\frac{\cosh\kappa_1 d\cosh\kappa_2 d}{\cosh\kappa_1 h\cosh\kappa_2 h}\right)\right.$$
$$\left.\left.-(\kappa_1^2+\kappa_2^2)\left(\tanh\kappa_1 h\tanh\kappa_2 h - \frac{\sinh\kappa_1 d}{\cosh\kappa_1 h}\frac{\sinh\kappa_2 d}{\cosh\kappa_2 h}\right)\right)\right\}. \tag{A7}$$

The case of $\kappa_1 = \kappa_2 = \kappa$ may occur in $\Gamma_4$, and we get

$$\Gamma_4(\kappa,\kappa) = \frac{1}{2}(\kappa h + \sinh\kappa h\cosh\kappa h) + \frac{1}{h+l}\left(-\kappa\frac{h^2-d^2}{4} + \frac{\cosh^2\kappa h - \cosh^2\kappa d}{4\kappa}\right). \tag{A8}$$

With reference to Equation (34) we only need $\Gamma_1$ for $(\kappa_1,\kappa_2) = (k_{jn} \pm k_{lm}^{-*}, K_p^{\pm})$. In terms of $D_{jnlm}^{\pm}$ defined in Equation (28b), we get

$$\Gamma_1(k_{jn} \pm k_{lm}^{-*}, K_p^{\pm}) = \frac{\cosh(k_{jn} \pm k_{lm}^{-*})h\cosh K_p^{\pm}h}{g((k_{jn} \pm k_{lm}^{-*})^2 - (K_p^{\pm})^2)} D_{jnlm}^{\pm}. \tag{A9}$$

Furthermore, $\Gamma_4$ appears as a function of $(\kappa_1,\kappa_2) = (k_{jn}, K_p^{\pm})$ for which we have

$$\Gamma_4(k_{jn}, K_p^{\pm}) = \frac{k_{jn}\cosh k_{jn}h \cosh K_p^{\pm}h}{k_{jn}^2 - (K_p^{\pm})^2}\left(\frac{\omega_n^2}{g} - \frac{(\omega_n \pm \omega_m)^2}{g} + \frac{M_2(k_{jn}, K_p^{\pm})}{g}\right), \tag{A10}$$

where

$$M_2(k_{jn}, K_p^{\pm}) \equiv -\frac{g}{h+l}\frac{K_p^{\pm}/k_{jn}}{k_{jn}^2 - (K_p^{\pm})^2}\left\{2k_{jn}K_p^{\pm}\left(1 - \frac{\cosh k_{jn}d \cosh K_p^{\pm}d}{\cosh k_{jn}h \cosh K_p^{\pm}h}\right)\right.$$
$$\left. - (k_{jn}^2 + (K_p^{\pm})^2)\left(\frac{(\omega_n \pm \omega_m)^2\omega_n^2}{g^2 k_{jn}K_p^{\pm}} - \frac{\sinh k_{jn}d \sinh K_p^{\pm}d}{\cosh k_{jn}h \cosh K_p^{\pm}h}\right)\right\} \tag{A11}$$

and where the dispersion relations (15) and (33) have been applied to reduce the number of hyperbolic functions.